AWARD NUMBER: W81XWH-16-1-0401

TITLE: Powering Up Mitochondrial Functions to Treat Mitochondrial Disease

PRINCIPAL INVESTIGATOR: Douglas Wallace, Ph.D.

CONTRACTING ORGANIZATION: Children's Hospital of Philadelphia
                                    Philadelphia, PA 19104

REPORT DATE: October 2017

TYPE OF REPORT: Annual

PREPARED FOR: U.S. Army Medical Research and Materiel Command
                        Fort Detrick, Maryland 21702-5012

DISTRIBUTION STATEMENT: Approved for Public Release;
                                    Distribution Unlimited

The views, opinions and/or findings contained in this report are those of the author(s) and should not be construed as an official Department of the Army position, policy or decision unless so designated by other documentation.

REPORT DOCUMENTATION PAGE			*Form Approved* OMB No. 0704-0188

Public reporting burden for this collection of information is estimated to average 1 hour per response, including the time for reviewing instructions, searching existing data sources, gathering and maintaining the data needed, and completing and reviewing this collection of information. Send comments regarding this burden estimate or any other aspect of this collection of information, including suggestions for reducing this burden to Department of Defense, Washington Headquarters Services, Directorate for Information Operations and Reports (0704-0188), 1215 Jefferson Davis Highway, Suite 1204, Arlington, VA 22202-4302. Respondents should be aware that notwithstanding any other provision of law, no person shall be subject to any penalty for failing to comply with a collection of information if it does not display a currently valid OMB control number. **PLEASE DO NOT RETURN YOUR FORM TO THE ABOVE ADDRESS.**

1. REPORT DATE	2. REPORT TYPE	3. DATES COVERED
October 2017	Annual	30 Sep 2016 – 29 Sep 2017

4. TITLE AND SUBTITLE

Powering Up Mitochondrial Functions to Treat Mitochondrial Disease

5a. CONTRACT NUMBER

5b. GRANT NUMBER
W81XWH-16-1-0401

5c. PROGRAM ELEMENT NUMBER

6. AUTHOR(S)
Douglas C. Wallace, Ph.D. and Liming Pei, Ph.D.

5d. PROJECT NUMBER

5e. TASK NUMBER

5f. WORK UNIT NUMBER

E-Mail: wallaced1@email.chop.edu and peil@email.chop.edu

7. PERFORMING ORGANIZATION NAME(S) AND ADDRESS(ES)
Children's Hospital of Philadelphia, The
3615 Civic Center Blvd
Philadelphia, PA 19104-4318

8. PERFORMING ORGANIZATION REPORT NUMBER

9. SPONSORING / MONITORING AGENCY NAME(S) AND ADDRESS(ES)

U.S. Army Medical Research and Materiel Command
Fort Detrick, Maryland 21702-5012

10. SPONSOR/MONITOR'S ACRONYM(S)

11. SPONSOR/MONITOR'S REPORT NUMBER(S)

12. DISTRIBUTION / AVAILABILITY STATEMENT

Approved for Public Release; Distribution Unlimited

13. SUPPLEMENTARY NOTES

14. ABSTRACT

We proposed that induction of the ERRα/γ signaling pathway can enhance mitochondrial function in both cell and animal models of mitochondrial disease. Our major findings include;
1) We recently compared in detail the different mitochondrial disease animal models (under review in Cell Metabolism). We found that the compound Ant1-/-ND6 mutant mouse model exhibited the earliest and strongest mitochondrial cardiomyopathy phenotype and therefore provided the best therapeutic window for our proposed intervention research strategy.
2) We discovered that GDF15 is a heart-derived hormone whose serum level correlates positively with the severity of mitochondrial cardiomyopathy (recently published with DOD grant support acknowledged), and it can be used as a biomarker in our studies.

15. SUBJECT TERMS
Mitochondria, mitochondrial disease, cardiomyopathy, estrogen-related receptor, transcriptional regulation, mitochondrial biogenesis, signaling, iPSCs, heart disease,

16. SECURITY CLASSIFICATION OF:			17. LIMITATION OF ABSTRACT	18. NUMBER OF PAGES	19a. NAME OF RESPONSIBLE PERSON USAMRMC
a. REPORT Unclassified	**b. ABSTRACT** Unclassified	**c. THIS PAGE** Unclassified	Unclassified	79	**19b. TELEPHONE NUMBER** *(include area code)*

Standard Form 298 (Rev. 8-98)
Prescribed by ANSI Std. Z39.18

Table of Contents

1. **INTRODUCTION:** We recently identified that two transcription factors, ERRα and ERRγ, are critical transcriptional regulators of mitochondrial biogenesis and function. Loss of both cardiac ERRα and ERRγ in mice results in severe mitochondrial cardiomyopathy, heart failure and death within the first month of life. This is because that ERRα and ERRγ are both sufficient and required to induce the transcription of many genes crucial for normal mitochondrial function and biogenesis. Overexpression of ERRα and ERRγ increases mitochondrial biogenesis and function in cells. Therefore, we hypothesize that induction of the ERRα/ERRγ signaling pathway (with both genetic and pharmacological approaches) can enhance mitochondrial function in both cells and tissues, thus providing a general approach for treating a broad spectrum of mitochondrial diseases. We propose to test our hypothesis using novel animal models of mitochondrial disease we recently developed.

2. **KEYWORDS:** Mitochondria, mitochondrial disease, cardiomyopathy, estrogen-related receptor, transcriptional regulation, mitochondrial biogenesis, signaling, iPSCs, heart disease

3. **ACCOMPLISHMENTS:**

   ▪ **What were the major goals of the project?**

Specific Aim 1 (specified in proposal)	Timeline	% complete	
Major Task 1	**Months**		
Subtask 1: Treat mitochondrial cardiomyopathy in ND6 mutant mice	1-36	30%; **Wallace lab** has generated mice; **Pei lab** is generating virus	
Subtask 2: Treat mitochondrial cardiomyopathy in CO1 mutant mice	1-36	30% **Wallace lab** has generated mice; **Pei lab** is generating virus	
Milestone(s) Achieved: Successful completion of subtasks 1 and 2.	36		

IACUC Approval	1	100% August 09, 2016 **Wallace and Pei**	
Milestone Achieved: HRPO/ACURO Approval	1	100% October 24, 2016 **Wallace and Pei**	
	Specific Aim 2 (specified in proposal)		
	Major Task 2		
Subtask 1: Treat mitochondrial cardiomyopathy in Ant1$_{-/-}$ mice	1-36	30% **Wallace lab** has generated mice; **Pei lab** is generating virus	
Milestone(s) Achieved: Successful completion of subtask 1.	36		
	Specific Aim 3 (specified in proposal)		
	Major Task 3		
Subtask 1: Improve mitochondrial and cellular functions in human Ant1$_{-/-}$ patient iPSCs-derived cardiomyocytes	13-36	10% **Pei lab**	
Milestone(s) Achieved: Successful completion of subtask 1	36		

What was accomplished under these goals?

1) Major activities: Overall we are on track to achieve our major research goals.

o Aims 1 and 2: the **Wallace lab** recently compared in detail the different mitochondrial disease animal models (under review in Cell Metabolism, also see Appendices). Based on these latest results we decided to prioritize our research efforts on the compound Ant1-/-ND6 mutant mouse model, because this model exhibited the earliest and strongest mitochondrial cardiomyopathy phenotype and therefore provided the best therapeutic window for our proposed intervention research strategy. We devoted our

efforts in this model in Year 1. The **Wallace lab** have set up breeding colonies that have generated the first cohort of compound Ant1-/-ND6 mutant mice for our experiments. The **Pei lab** is generating the AAV9-ERRγ virus and the **Pei lab** expects to inject Ant1-/-ND6 mutant mice in the first 2 months of Year 2.

- o Aim 3: **Pei lab** has initiated studies in Aim 3 using Ant1-/- iPSC. We have designed and adopted a new gene-editing approach to overexpress ERRγ in control and Ant1-/- iPSC and differentiated cardiomyocytes. This improved approach will also allow us to control the timing and scale of ERRγ overexpression.

2) Specific objectives: In addition to aforementioned progress in major activities, **Pei and Wallace** together have successfully achieved milestones of institute IACUC protocol and ACURO approvals on time.

3) Significant results and key outcomes:

- o **Pei lab** has recently discovered that GDF15 is a heart-derived hormone that regulates body growth. Circulating GDF15 level correlates positively with the severity of mitochondrial cardiomyopathy and can be used as a serum biomarker for our mitochondrial disease studies. This work was recently published (see appendices) and the DOD grant support was acknowledged. We will take advantage of these new findings and monitor serum GDF15 level as an additional, more convenient and less invasive method to determine whether mitochondrial cardiomyopathy was ameliorated by ERR overexpression and activation (Aims 1 and 2).

- o **Wallace lab** recently compared in detail the different mitochondrial disease animal models (under review in Cell Metabolism, also see Appendices). We found that the compound Ant1-/-ND6 mutant mouse model exhibited the earliest and strongest mitochondrial cardiomyopathy phenotype and therefore provided the best therapeutic window for our proposed intervention research strategy.

- ▪ **What opportunities for training and professional development has the project provided?**

- Training: Dr. Zhao has received one-on-one training in iPSC technology and gene editing.

- Professional Development: Dr. **Wallace**, **Pei,** Murdock, Hernandez, and Zhao all attended The TriMAD Regional Symposium in 2016. TriMAD is an annual conference which promotes cross-talk and collaboration between mitochondrial/metabolism and aging-centered research groups at the University of Pittsburgh, Penn State, and the University of Pennsylvania, and CHOP.

- **How were the results disseminated to communities of interest?**

- The **Pei lab** has published a manuscript showing that GDF15 is a heart-derived hormone that regulated body growth. (Wang T, McDonald C, Lupino K, Zhai X, Wilkins BJ, Hakonarson H, Pei L. 2017 EMBO Mol Med 2017 Aug;9(8): 1150-1164, see appendix)

- The **Wallace lab** has a manuscript in review at Cell Metabolism that described the cardiac phenotype of mice with combined mutations in mitochondrial and nuclear genes. (McManus M, Chen HW, Picard M, DeHaas HJ, Potluri P, Leipzig J, Towheed A, Angelin A, Sengupta P, Morrow R, Kauffman B, Vermulst M, Narula J, Wallace DC. 2017 Mitochondrial DNA Variation Dictates Expressivity and Progression of Nuclear DNA Mutations Causing Cardiomyopathy, in review)

- **What do you plan to do during the next reporting period to accomplish the goals?**

  We plan to make significant progress in all research aims. For Aims 1 and 2, the **Wallace** lab will continue to breed and genotype the mitochondrial mutant mice needed, and to provide expertise in their care and evaluation. The **Pei** hopes to complete injecting AAV9-ERR to all Ant1-/-ND6 mutant mice, and the **Pei lab** will monitor their cardiac functions periodically as we proposed. For Aim 3 the **Pei lab** hopes to complete establishing the ERR overexpressing Ant1-/- iPSC and differentiated cardiomyocytes, and the **Pei lab** and **Wallace lab** will proceed with evaluating all different aspects of their mitochondrial and cardiac functions as we proposed.

  4. **IMPACT:**

- **What was the impact on the development of the principal discipline(s) of the project?**

  The **Pei lab** recently discovered that GDF15 is a heart-derived hormone that regulates body growth. Circulating GDF15 level correlates positively with the severity of mitochondrial cardiomyopathy and can be used as a serum biomarker for our

mitochondrial disease studies. This work was recently published (see appendices) and the DOD grant support was acknowledged. We will take advantage of these new findings and monitor serum GDF15 level as an additional, more convenient and less invasive method to determine whether mitochondrial cardiomyopathy was ameliorated by ERR overexpression and activation (Aims 1 and 2).

- **What was the impact on other disciplines?**

  The **Pei lab** recently discovered that GDF15 is a heart-derived hormone that regulates body growth. Pediatric heart disease induces GDF15 synthesis and secretion by cardiomyocytes. Circulating GDF15 in turn acts on the liver to inhibit growth hormone (GH) signaling and body growth. We demonstrate that blocking cardiomyocyte production of GDF15 normalizes circulating GDF15 level and restores liver GH signaling, establishing GDF15 as a bona fide heart-derived hormone that regulates pediatric body growth. Importantly, plasma GDF15 is further increased in children with concomitant heart disease and failure to thrive (FTT). Together these studies reveal a new endocrine mechanism by which the heart coordinates cardiac function and body growth. Our results also provide a potential mechanism for the well-established clinical observation that children with heart diseases often develop FTT. This work was recently published (see appendices) and the DOD grant support was acknowledged.
- **What was the impact on technology transfer?**
- Nothing to Report
- **What was the impact on society beyond science and technology?**
  - Nothing to report

5. **CHANGES/PROBLEMS:**
- **Changes in approach and reasons for change**
- As detailed above, we have prioritized the compound Ant1-/-ND6 mutant mouse model based on our latest research results. This model exhibited the earliest and strongest mitochondrial cardiomyopathy phenotype and therefore provided the best therapeutic window for our proposed intervention research strategy. We devoted our efforts in this model in Year 1 and moving forward.
- **Changes that had a significant impact on expenditures**
- Nothing to report
- **Significant changes in use or care of human subjects, vertebrate animals, biohazards, and/or select agents**

- Nothing to report
- **Significant changes in use or care of human subjects**
- Nothing to report
- **Significant changes in use or care of vertebrate animals.**
- Nothing to report
- **Significant changes in use of biohazards and/or select agents**
- Nothing to report

6. **PRODUCTS:**
- **Publications, conference papers, and presentations**
  - **Journal publications.**

    Wang T, Liu J, McDonald, C, Lupino K, Zhai X, Wilkins BJ, Hakonarson H, **Pei L** (2017). GDF15 is a heart-derived hormone that regulates body growth. EMBO Molecular Medicine 9, 1150-1164. PMID: 28572090. PMCID: PMC5538424. (published, DOD support acknowledged).

    McManus MJ, Chen HW, Picard M, Potluri P, Leipzig J, Towheed A, Angelin A, Sengupta P, Morrow R, Kauffman B, Vermulst M, Narula J, Wallace DC. (in revision) Mitochondrial DNA Variation Dictates Expressivity and Progession of Nuclear DNA Mutations Causing Cardiomyopathy. Cell Metabolism in revision

  - **Books or other non-periodical, one-time publications.** Nothing to report
  - **Other publications, conference papers, and presentations.**
  - **Liming Pei presentations**

*10/2016   The 6th Regional Translational Research in Mitochondrial, Aging, and Disease (TriMAD) Symposium. Philadelphia, PA. "Listen to your heart"

*05/2017   Keystone Symposia—Mitochondria, Metabolism and Heart. Santa Fe, NM. "A heart-derived hormone that regulates body growth"

*05/2017   Cold Spring Harbor Laboratory meetings—Mechanisms of Metabolic Signaling. Cold Spring Harbor, NY.

09/2017   Inaugural Canadian Mitochondrial Disease Conference Toronto, Canada. "Regulation of mitochondrial function by nuclear receptors"

10/2017   Institute for Diabetes and Obesity (IDO), Helmholtz Zentrum München, Munich, Germany "Listen to your heart – a heart-derived hormone that regulates body growth"

Doug Wallace presentations

Oct, 2016   "A Mitochondria Etiology of Complex Diseases", The 19th Annual John B. Little Symposium – Theme: "Using Innovative Approaches in Stress Response Research", Boston, MA

Nov, 2016   "A Mitochondria Etiology of Complex Diseases", The 11th Annual International Conference on Genomics, Shenzhen, China

Nov, 2016   "A Mitochondria Etiology of Complex Diseases", The Seminars in Neuroscience: Brain, Mind, and Society Lecturer Series, Vanderbilt University, Nashville, TX

Nov, 2016   "A Mitochondria Etiology of Complex Diseases", University of California, San Francisco, San Francisco, CA

Dec, 2016   "A Mitochondrial Etiology of Complex Diseases", 2nd Conference Functional Genomics and Beyond: Nature via Nurture, Qatar National Convention Center, Doha, Qatar

Jan, 2017   "A Mitochondrial Etiology of Ophthalmological Diseases", Basic Science Course in Ophthalmology at Columbia University, New York, NY

Feb, 2017   "A Mitochondrial Etiology of Common Complex Diseases", Wayne State Seminar, Detroit, MI

Feb, 2017   "A Mitochondria Etiology of Complex Diseases", Temple University School of Medicine, Philadelphia, PA

Mar, 2017   "A Mitochondria Etiology of Complex Diseases", Oregon Health & Science University, Combined Basic Science Seminar, Portland, OR

Mar, 2017   "A Mitochondria Etiology of Complex Diseases", East Carolina Diabetes and Obesity Institute, Greenville, NC

May, 2017   "Human Origins and Complex Diseases: A Mitochondrial Perspective", The 2017 Franklin Institute Life Science Symposium 'Mitochondria: Our Origins – Our Diseases', The College of Physicians of Philadelphia, PA

May, 2017   "A Mitochondrial Etiology of Common Complex Diseases", The Florida Hospital Research Forum, Orlando, FL

May, 2017   "A Mitochondrial Etiology of Common Complex Diseases", Clinical and Translational Science Institute (CTSI) Seminar at UCLA Luskin, Los Angeles, CA

June, 2017 "Mitochondrial DNA Variation: Its Origins and Impact on Health", 27th Marabou Nutrition Conference, Stockholm, Sweden

June, 2017 "Mitochondrial Physiology and Molecular Genetics of Human Origins and Diseases", MBL Physiology Lecture, Woods Hole, MA

July, 2017 "A Mitochondrial Eitology of Neuropsychiatric Disorders", Collaborate2Cure, Philadelphia, PA

Aug, 2017 "Mitochondrial in Human Evolution and Disease", University of Pennsylvania Perelman School of Medicine, Undergraduate Student Scholar Programs Symposium, Philadelphia, PA

Sept, 2017 "Mitochondrial DNA Variation in Human Evolution and Disease", Mitochondrial Evolutionary Genomics Conference Keynote Speaker, Ein Gedi, Israel

Sep, 2017 "The Mitochondrion: Our Origins – Our Diseases", 2017 Dr. Paul Janssen Award Symposium, New York City, NY

Sep, 2017 "A Mitochondrial Etiology of Metabolic and Degenerative Diseases", The Canada Mitochondrial Network and MitoCanada Foundation, Toronto, Canada

Oct, 2017 "The Mitochondrion: Our Origins – Our Diseases", Genetics and Complex Diseases, Harvard Chan School, Boston, MA

Oct, 2017 "A Mitochondrial Etiology of Complex Diseases", University of Pennsylvania Perelman School of Medicine, Department of Cardiovascular Institute Seminar Series, Philadelphia, PA

Oct, 2017 "Mitochondria: Our Origins-Our Diseases", Cornell University, Ithaca, NY

Oct, 2017 "Our Origins-Our Diseases: The Mitochondrial Perspective", Golden Sages Lecture, Bryn Mawr College, Bryn, Mawr, PA

Oct, 2017 "A Mitochondrial Etiology of Complex Diseases and Associated Inflammation", University of Pennsylvania Perelman School of Medicine, Penn Transplant Institute Research Lecture, Philadelphia, PA

Oct, 2017 "Mitochondria: Our Origins-Our Diseases", the 12th Annual International Conference in Genomics, Shenzhen, China

Nov, 2017 "Mitochondrial Variation in Metabolic and Degenerative Diseases, Cancer, & Aging", University of Chicago Cancer Biology Seminar Series, Chicago, IL

Nov, 2017 "Mitochondrial Genetic Variation in Human Evolution and Disease", Cleveland Clinic, Cleveland, OH

- **Website(s) or other Internet site(s)**

  www.mitomap.org

MITOMAP reports published and unpublished data on human mitochondrial DNA variation. Currently our variant tables report frequencies from 30589 human mitochondrial DNA sequences.

- **Technologies or techniques**

  nothing to report

- **Inventions, patent applications, and/or licenses**

  nothing to report

- **Other Products**

  nothing to report

7. **PARTICIPANTS & OTHER COLLABORATING ORGANIZATIONS**

- **What individuals have worked on the project?**

Name:	***Douglas C. Wallace, Ph.D.***
Project Role:	*No change*
Name:	***Deborah G. Murdock, Ph.D.***
Project Role:	*No change*
Name:	***Jesus Tintos Hernandez, Ph.D.***
Project Role:	*Postdoctoral fellow*
Nearest person month worked:	*3*
Contribution to Project:	*Dr. Hernandez has been instrumental in creation and maintenance of iPSCs*
Name:	***Danielle Rittenhouse, BS***
Project Role:	*Research Technician*
Nearest person month worked:	*4*
Contribution to Project:	*Ms Rittenhouse replaced Katelyn Sweeney as the research technician responsible for mouse husbandry.*
Name:	***Arrienne Butic, BS***

Project Role:	*Research technician*
Nearest person month worked:	*1*
Contribution to Project:	*Ms Butic has replaced D Rittenhouse as the research technician responsible for mouse husbandry.*

- **Has there been a change in the active other support of the PD/PI(s) or senior/key personnel since the last reporting period?** See below

RESEARCH SUPPORT DOUGLAS WALLACE

ACTIVE SUPPORT

5R01-NS021328-30 (PI D. Wallace)   04/01/13 – 03/31/18   1.2 calendar months

National Institutes of Health (NIH) $261,528

Mitochondrial Inborn Errors of Metabolism

This project will investigate the genetics of maternally inherited neurological diseases.

Role: PI

There is no scientific or budgetary overlap

100041003 (PI D. Wallace)   10/01/14 – 12/31/17   0.24 calendar months

GlaxoSmithKline
$119,048

Mitochondria and Chronic Obstructive Pulmonary Disease: A LHON Connection

This project will investigate how mtDNA cybrids can be used to test the efficacy of increasing antioxidant defenses by activation of Nrf2 of reducing mtDNA oxidative damage by over expression of OGG1.

Role: PI

There is no scientific or budgetary overlap

N/A (PI Atif Towheed/D. Wallace)   07/01/15 – 07/31/18 1.2 calendar months

United Mitochondrial Disease Foundation $35,000

Allotopic RNA Rescue of LHON Mouse Models

This project will investigate the use of a novel gene therapy approach in correcting the mutant phenotype in a LHON mouse model

Role: Fellowship Grant

There is no scientific or budgetary overlap

This grant has been extended

R01OD010944-05 (PI M. Alexeyev)   01/01/16 – 11/30/20   0.24 calendar months

National Institutes of Health (NIH) $101,250

Generation and Characterization of Mouse Models of mtDNA Mutations

This project is involved in generating new mouse mtDNA Mutations models of tRNA Disease

Role: Co-PI

There is no scientific or budgetary overlap

1R01MH108592-01A1 (PI D. Wallace)   07/01/16 – 06/30/21   1.2 calendar months

National Institutes of Health (NIH) $400,773

A Mitochondrial-Interneuronal Hypothesis of Autism

This project will investigate mitochondrial defect-interneuron imbalance as a

major contributor to autism spectrum disorder (ASD) risk.

Role: PI

There is no scientific or budgetary overlap

This grant started

SparkTherapeutics (Douglas Wallace) 09/1/2016 – 08/31/18 0.36 calendar months

AAV-Mediated Gene Therapy for LHON $503,673

This project will investigate the use of AAV- mediated gene therapy in mice.

Role: PI

There is no scientific or budgetary overlap

This grant started

PR150585   Pei and Wallace Partner PI's 09/30/16 – 09/29/1 1.2 calendar months
         Department of Defense
         $250,000

Powering Up Mitochondrial Function to Treat Mitochondrial Disease

This project is to determine whether induction of the ERR pathway can be employed as a novel approach to treat mitochondrial disease in a preclinical model.

Role: Co-PI

There is no scientific or budgetary overlap

This grant started

1R01MN110185-01A1 Anderson (PI) 09/20/16 – 08/31/19   0.6 calendar months

National Institutes of Health (NIH) $354,894

IPSC phenotype, mitochondrial haplotype and psychosis in 22q11 deletion syndrome

The goal of this proposal is to test the hypothesis that, in 22q11 deletion syndrome, a "second hit" within mitochondria-related genes increases metabolic dysfunction in neurons and is associated with an sed risk of schizophrenia in patients.

Role: Co-Investigator

There is no scientific or budgetary overlap

This grant started

RO1 DK111495 (Pei)   9/30/2016 – 9/29/2022   0.24 calendar months
National Institutes of Health (NIH) $250,000
Coordinated regulation of mitochondrial and cellular functions by nuclear receptors.
The major goal of this project is to determine mechanistically how nuclear receptors especially ERRγ coordinately regulate mitochondrial and cellular functions in kidney biology and disease.
Role: Co- Investigator
There is no scientific or budgetary overlap

This grant started

RO1 GM124532-01 (Vermulst) 08/01/2017 – 07/31/2021   0.36 calendar months
National Institutes of Health (NIH) $192,500
Targeting the IGF-1/insulin signaling pathway to treat mtDNA
This proposal will test in yeast and mice the hypothesis that the aggregation of certain proteins can be
triggered by errors that occur during transcription.
Role: Co- Investigator

There is no scientific or budgetary overlap

This grant started

NIH 1U2CHL138346-01 (PI Resnick)7/1/2017 – 6/30/2022 0.24 calendar months

National Institutes of Health (NIH) $2,564,629

U2C Kids First Pediatric Data Resource Center

The Kids First Data Resource will 1) serve as a centralized data hub to integrate dispersed data sources and provide harmonized data sets 2) provide easy access to and querying of disparate data sets via a web portal for researchers without bioinformatics expertise 3) provide tools for analyzing large and complex data sets encompassing genetic sequence and clinical data.

Role: Co- Investigator

There is no scientific or budgetary overlap

This grant started

NIH 1U24HD093483-01   (PI Falk) 8/23/2017 – 5/31/2020   0.12 calendar months

National Institutes of Health (NIH) $202,056

Expert Curation Panel (U24) Mitochondrial Leigh Syndrome

The goal of the grant is to establish an expert panel curation of disease-gene and gene variant pathogenicity assertions and clinical actionability for the most prevalent of treatable genetic causes of Leigh syndrome and related pediatric mitochondrial disorders causing severe neurodevelopmental disabilities.

Role: Co-Investigator

There is no scientific or budgetary overlap

This grant started

SUPPORT

Deborah Murdock

<u>ACTIVE</u>

1R01MH108592-01A1 (PI D. Wallace)   07/01/16 – 06/30/21 3.0 calendar months

National Institutes of Health (NIH) $261,528

A Mitochondrial-Interneuronal Hypothesis of Autism,

This project will investigate mitochondrial defect-interneuron imbalance as a major contributor to autism spectrum disorder (ASD) risk.

Role: Senior Scientist

There is no scientific or budgetary overlap

This grant started

Spark Therapeutics (Douglas Wallace) 09/1/2016 – 08/31/18 3.6 calendar months

AAV-Mediated Gene Therapy for LHON $503,673

This project will investigate the use of AAV- mediated gene therapy in mice.

Role: Senior Scientist

There is no scientific or budgetary overlap

This grant started

PR150585   Pei and Wallace Partner PI's 09/30/16 – 09/29/18 3.0 calendar months

Department of Defense $250,000

Powering Up Mitochondrial Function to Treat Mitochondrial Disease

This project is to determine whether induction of the ERR pathway can be employed as a novel approach to treat mitochondrial disease in a preclinical model.

Role: Senior Scientist

There is no scientific or budgetary overlap

1R01MN110185-01A1 Anderson (PI)   09/20/16 – 08/31/19 1.2 calendar months
National Institutes of Health (NIH) $354,894

IPSC phenotype, mitochondrial haplotype and psychosis in 22q11 deletion syndrome

The goal of this proposal is to test the hypothesis that, in 22q11 deletion syndrome, a "second hit" within mitochondria-related genes increases metabolic dysfunction in neurons and is associated with an increased risk of schizophrenia in patients.
Role: Senior Scientist

There is no scientific or budgetary overlap

This grant started

RO1 (Vermulst)   08/01/2017 – 07/31/2021   1.2 calendar months
National Institutes of Health (NIH) $192,500
Targeting the IGF-1/insulin signaling pathway to treat mtDNA

This proposal will test in yeast and mice the hypothesis that the aggregation of certain proteins can be triggered by errors that occur during transcription.
Role: Senior Scientist
There is no scientific or budgetary overlap

This grant started

What other organizations were involved as partners?

Nothing to Report

Cell Metabolism

Mitochondrial DNA Variation Dictates Expressivity and Progression of Nuclear DNA Mutations Causing Cardiomyopathy

--Manuscript Draft--

Manuscript Number:	
Full Title:	Mitochondrial DNA Variation Dictates Expressivity and Progression of Nuclear DNA Mutations Causing Cardiomyopathy
Article Type:	Research Article
Keywords:	mitochondrial-nuclear interaction; mitochondrial DNA; adenine nucleotide translocator; ANT1; complex I; complex IV; F1Fo-ATPase; mtDNA instability; cardiomyopathy; aging; mitochondrial ultrastructure
Corresponding Author:	Douglas C. Wallace Children's Hospital of Philadelphia Philadelphia, PA UNITED STATES
First Author:	Meagan J. McManus
Order of Authors:	Meagan J. McManus
	Hsiao-Wen Chen
	Martin Picard
	Hans J. De Haas
	Prasanth Potluri
	Jeremy Leipzig
	Atif Towheed
	Alessia Angelin
	Partho Sengupta
	Ryan Morrow
	Brett Kauffman
	Marc Vermulst
	Jagat Narula
	Douglas C. Wallace
Abstract:	Nuclear-encoded mutations causing metabolic and degenerative diseases have highly variable phenotypic expression. Patients sharing the homozygous mutation (c.523delC) in the adenine nucleotide translocator 1 gene (SLC25A4, ANT1) develop cardiomyopathy that varies from slowly progressive to fulminant. This variability correlates with the mitochondrial DNA (mtDNA) lineage. To confirm that mtDNA variants can modulate the expressivity of nuclear DNA (nDNA)-encoded diseases, we combined in mice the nDNA Slc25a4-/- null mutation with a homoplasmic mtDNA ND6P25L or COIV421A variant. The ND6P25L variant significantly increased the severity of cardiomyopathy while the COIV421A variant was phenotypically neutral. The adverse Slc25a4-/- and ND6P25L combination was associated with impaired mitochondrial complex I activity, altered mitochondrial morphology, increased reactive oxygen species production, sensitization of the mitochondrial permeability transition pore, increased somatic mtDNA mutation levels, and shortened lifespan. The strikingly different phenotypic effects of these mild mtDNA variants demonstrate that mtDNA can be an important modulator of autosomal disease.
Suggested Reviewers:	Vincent Procaccio,, M.D., Ph.D. Professor Departments of Biochemistry and Genetics, National Center for Neurodegenerative and Mitochondrial diseases CHU Angers ViProcaccio@chu-angers.fr

	Dr. Procaccio codirects the mitochondrial disease unit in Angers, France, is a mitochondrial medicine clinician, and has been studying mutations in both nDNA and mtDNA mutations that cause mitochondrial diseases since the late 1980s. He is highly knowledgeable about the clinical variability associated with these diseases.
	Michael Zaragoza, M.D., Ph.D. Professor, School of Medicine University of California, Irvine mzaragoz@uci.edu Dr. Zaragoza is an American clinical geneticist who has published on both the clinical effects of ANT1 mutations and on the complexities of interpreting the pathogenicity of mtDNA mutations.
	Saleh M. Ibrahim, Ph.D. University of Lübeck Saleh.Ibrahim@uksh.de Dr. Ibrahim is internationally recognized for his work developing conplastic mouse stains with identical nuclei but different mtDNAs. He has shown that naturally occurring mtDNA variation can significantly affect the phenotypes of "wildtype" mice.
	Valerio Carelli, MD, PhD Chief of the Laboratory of Neurogenetics, University of Bologna School of Medicine valerio.carelli@unibo.it Dr. Carelli is a leading Italian Mitochondrial Clinician who has published extensively on how "normal" mtDNA polymorphic variants can interact with pathogenic mtDNA variants to modulate the severity of the phenotype.
Opposed Reviewers:	

The Children's Hospital
of Philadelphia®

RESEARCH INSTITUTE

CENTER FOR MITOCHONDRIAL
AND EPIGENOMIC MEDICINE

Douglas C. Wallace, Ph.D.
Michael and Charles Barnett Endowed Chair in Pediatric
Mitochondrial Medicine and Metabolic Disease
Professor and Director
3501 Civic Center Blvd., CTRB 6060
Philadelphia, PA 19104
Phone: 267-425-3034
WallaceD1@email.chop.edu

June 21, 2017

Anne Granger, Ph.D.
Scientific Editor
Cell Metabolism

Dear Dr. Granger:

My colleague, Dr. Meagan McManus, indicated how pleased she was to reconnect with you at the meeting last week in Sweden. At the meeting, you expressed interest in her poster reporting our mouse genetic experiments on the role of mitochondrial DNA (mtDNA) variation in regulating the expressivity of pathogenic nuclear DNA (nDNA) gene mutations. Following up on your discussions, we would like to ask if you would consider for publication in *Cell Metabolism* our manuscript titled, "**Mitochondrial DNA Variation Dictates Expressivity and Progression of Nuclear DNA Mutations Causing Cardiomyopathy**" by Meagan J. McManus and collaborators.

Degenerative diseases resulting from autosomal "Mendelian" gene mutations frequently have variable clinical manifestions and a delayed onest and progressive course. However, nothing in the deterministic principles of Mendelian genetics predicts these common phenomena. The *ad hoc* assumption has been that the variability in Mendelian phenotypes is due to the interaction of multiple nuclear genes. However, even if true, this still does not explain why a Mendelian disease mutation would be delayed in expression until adulthood. In the associated manucript we show that these non-Mendelian-like behaviors are the result of mtDNA variation.

Previously, we reported a human pedigree in which the patients suffered from cardiomyopathy due to a recessive mutation in the nDNA *SLC25A4* gene. While all homozygous mutant family members had hypertrophic cardiomyopathy, some family members had mild hypertrophic cardiomyopathy while others with the same nDNA genotype had fulminating dilated cardiomyopathy requiring heart transplant. Further analysis of these patients revealed that the severity of the homozygous nDNA mutation correlated with the mtDNA lineage. mtDNA haplogroup H was associated with mild cardiomyopathy while haplogroup U was associated with severe cardiomyopathy. While this correlation suggested that the mtDNA lineage was the determining factor for cardiomyopathy severity, it was not proof and the mechanism by which mtDNA variation modulated nDNA gene mutant phenotypes was not elucidated.

To rectify these deficiencies, we have modeled this human disease in the mouse. We combined our mouse nDNA *Slc25A4* homozygous mutation with two of our mouse mtDNA mutations, one in a mitochondrial complex I gene ($ND6^{P25L}$) and the other in a complex IV gene (COI^{V421A}). Analysis of these mouse genetic combinations revealed that the $Slc25A4$-$ND6^{P25L}$ combination resulted in severe cardiomyopathy, reducing the lifespan by half, while the $Slc25A4$-COI^{V421A} combination resembled the $Slc25A4$ mutation with normal mtDNA. Further analysis revealed that both the $Slc25A4$ and $ND6^{P25L}$ mutations impaired respiratory complex I, though in different ways. By contrast, the COI^{V421A} mutation partially compensated for the $Slc25A4$ complex I defect. Hence, mtDNA variation does modulate the pathophysiology of nDNA mutations accounting for the variable expressivity.

But what about the delayed onset and progressive course? Each cardiomyocyte contains thousands of mtDNAs which replicate throughout life. We hypothesized that mutations accumulate in the cardiomyocyte mtDNAs which age further eroding mitochondrial energetics until energy insufficiency results in cardiac failure. To determine if this was the case, we quantified the somatic mtDNA mutation levels in the different mouse strains and found that the *Slc25A4-ND6*^{P25L} strain with the shortest lifespan had the highest rate of somatic mtDNA mutation accumulation. Thus the accumulation of somatic mtDNA mutations explains the delayed onset and progressive course of disease.

In conclusion, mtDNA variation can explain the seemingly aberrant behaviors of classical Mendelian disease genes. Hence, characterization of mtDNA variation should be an important adjunct to studies on nDNA diseases.

Should you decide to have this paper reviewed, we would like to suggest the following individuals as possible referees:

Vincent Procaccio, M.D., Ph.D.
Professor Departments of Biochemistry and Genetics
National Center for Neurodegenerative and Mitochondrial diseases
CHU Angers
4 rue Larrey, 49933 Angers, France
UMR CNRS 6214 – INSERM U1083
Mitochondrial and NeuroVascular Biology
Phone 33 2 41 35 78 54
Email: ViProcaccio@chu-angers.fr

Michael V. Zaragoza, M.D., Ph.D.
Departments of Pediatrics-Genetics & Genomics Division & Biological Chemistry
School of Medicine
University of California, Irvine
2042 Hewitt Hall
Mail Code: 3940
Irvine, CA 92697
Phone: (949) 824-8813
Email: mzaragoz@uci.edu

Saleh M. Ibrahim, Ph.D.
Lübeck Institute of Experimental Dermatology,
University of Lübeck,
Lübeck, D-23562, Germany
Email: Saleh.Ibrahim@uksh.de

Valerio Carelli, MD, PhD
Tenure Permanent Researcher
Chief of the Laboratory of Neurogenetics,
Department of Biomedical and NeuroMotor Sciences (DIBINEM),
University of Bologna School of Medicine,
Ospedale Bellaria (Pad. G), Via Altura 3, 40139 Bologna.
Phone: ++39 051 4966747
FAX : ++39 051 209 2751
Email: valerio.carelli@unibo.i

Thank you for your consideration.

Sincerely yours,

Douglas C. Wallace, Ph.D.
Michael and Charles Barnett Endowed Chair in Pediatric Mitochondrial Medicine and Metabolic Disease
Director, Center of Mitochondrial and Epigenomic Medicine, Children's Hospital of Philadelphia

Mitochondrial DNA Variation Dictates Expressivity and Progression of Nuclear DNA Mutations Causing Cardiomyopathy

Meagan J McManus[1], Hsiao-Wen Chen[1], Martin Picard[1], Hans J. De Haas[3], Prasanth Potluri[1], Jeremy Leipzig[1], Atif Towheed[1], Alessia Angelin[1], Partho Sengupta[3], Ryan M. Morrow[1], Brett A. Kauffman[4], Marc Vermulst[1], Jagat Narula[3], Douglas C. Wallace[1,2]

[1] Center for Mitochondrial and Epigenomic Medicine, The Children's Hospital of Philadelphia and University of Pennsylvania, Philadelphia, PA, 19104, USA

[2] Department of Pathology and Laboratory Medicine, University of Pennsylvania, Philadelphia, PA, 19104, USA

[3] Department of Medicine, Mount Sinai Hospital, New York, NY, 10029, USA

[4] Vascular Medicine Institute, University of Pittsburgh, Pittsburgh, PA, 15261, USA

Running head: mtDNA dictates expressivity of nDNA cardiomyopathy

Correspondence:
Douglas C. Wallace, Ph.D.
Michael and Charles Barnett Chair in Pediatric Mitochondrial Medicine and Metabolic Disease
Director, Center of Mitochondrial and Epigenomic Medicine, Children's Hospital of Philadelphia
Professor of Pathology and Laboratory Medicine, University of Pennsylvania
Colket Translational Research Building, room 6060
3501 Civic Center Boulevard, Philadelphia, PA 19104-4302
E-mail: wallaced1@email.chop.edu
Phone: 1-267-425-3034
Fax: 267-426-0978

Summary

Nuclear-encoded mutations causing metabolic and degenerative diseases have highly variable phenotypic expression. Patients sharing the homozygous mutation (c.523delC) in the adenine nucleotide translocator 1 gene (*SLC25A4, ANT1*) develop cardiomyopathy that varies from slowly progressive to fulminant. This variability correlates with the mitochondrial DNA (mtDNA) lineage. To confirm that mtDNA variants can modulate the expressivity of nuclear DNA (nDNA)-encoded diseases, we combined in mice the nDNA *Slc25a4*$^{-/-}$ null mutation with a homoplasmic mtDNA *ND6*^{P25L} or *COI*^{V421A} variant. The *ND6*^{P25L} variant significantly increased the severity of cardiomyopathy while the *COI*^{V421A} variant was phenotypically neutral. The adverse *Slc25a4*$^{-/-}$ and *ND6*^{P25L} combination was associated with impaired mitochondrial complex I activity, altered mitochondrial morphology, increased reactive oxygen species production, sensitization of the mitochondrial permeability transition pore, increased somatic mtDNA mutation levels, and shortened lifespan. The strikingly different phenotypic effects of these mild mtDNA variants demonstrate that mtDNA can be an important modulator of autosomal disease.

Keywords: mitochondrial-nuclear interaction, mitochondrial DNA, adenine nucleotide translocator, ANT1, complex I, complex IV, F_1F_o-ATPase, mtDNA instability, cardiomyopathy, aging, mitochondrial ultrastructure

Introduction

Mitochondrial dysfunction may play a critical role in the pathophysiology of complex metabolic and degenerative diseases (Wallace, 2013b; Wallace et al., 2013). One such disease is cardiomyopathy, in which mitochondrial dysfunction has been demonstrated in both pediatric and adult cases (Murphy et al., 2016; Porter et al., 2011; Zaragoza et al., 2011).

The mitochondrial proteome is encoded by 1,000 to 2,000 nDNA genes and by hundreds to thousands of copies of the maternally-inherited mtDNA. The mtDNA encodes for 13 essential polypeptides required for energy production via oxidative phosphorylation (OXPHOS). The energetically favorable transfer of electrons through OXPHOS complexes I-IV is used to generate an electrochemical gradient across the mitochondrial inner membrane that is utilized by complex V (H$^+$-pumping F_1,F_0 ATP synthase) to produce ATP. Mitochondrial matrix ATP is then exchanged for cytosolic ADP by the inner membrane adenine nucleotide translocators (ANTs). In addition to ATP/ADP translocation, the ANTs regulate the mitochondrial permeability transition pore (mtPTP) in distinct ways depending upon the isoform (Bauer et al., 1999; Chevrollier et al., 2011; Jang et al., 2008; Kokoszka et al., 2004; Zamora et al., 2004a; Zamora et al., 2004b). Humans have four ANT isoforms, while mice have three, but both species express the heart–muscle-brain isoform, ANT1 (*SLC25A4*), and the systemic isoform, ANT2 (*SLC25A5*), in the heart (Kokoszka et al., 2016). Hence, inactivation of the *SLC25A4* gene will result in a partial cardiac ANT defect.

Inactivating mutations in *ANT1* cause autosomal recessive myopathy and cardiomyopathy (Echaniz-Laguna et al., 2012; Palmieri et al., 2005). However, the severity of ANT1-deficient cardiomyopathy can be variable and this variability has been correlated with the mtDNA lineage (Strauss et al., 2013).

There are three types of clinically relevant mtDNA variation: functional polymorphisms which are associated with ancient mtDNA lineages called haplogroups, recent deleterious mutations that can result in maternally-inherited disease, and somatic mutations that accumulate in tissues over time. The phenotypic consequences of these different types of mtDNA variation are interdependent (Ji et al., 2012) and may be modulated by interactions with nDNA variants, as well as the environment (Wallace, 2013a). Due to these complex interactions, the etiological significance of mtDNA variation in common, age-related diseases has been difficult to delineate (Zaragoza et al., 2011). Therefore, the significance of mtDNA contribution to cardiomyopathy in which patients harbour mtDNA variants along with nDNA contractile protein mutations (Arbustini et al., 1998a; Arbustini et al., 1998b), or *ANT1* mutations (Strauss et al., 2013), remains to be clarified.

To address this knowledge gap, we have developed a mouse model of mitochondrial cardiomyopathy by combining the *Slc25a4* (*Ant1*) null gene mutation (Graham et al., 1997; Narula et al., 2011) with two different mild mtDNA variants. These mtDNA variants are the NADH dehydrogenase subunit 6 (*ND6*) gene nucleotide 13997G>A missense mutation (*ND6*[P25L]) causing a partial complex I defect (Lin et al., 2012) and the cytochrome c oxidase subunit 1 gene (*COI*) nucleotide 6589 T>C missense mutation (*COI*[V421A]) that results in a partial defect in complex IV activity (Fan et al., 2008).

Here we report the physiological effects of six nDNA-mtDNA combinations of wild type and mutant nDNA *Ant1* and mtDNA *COI*[V421A] and *ND6*[P25L] alleles in C57Bl/6JEiJ mice (Navarro et al., 2012). This investigation has established that mild differences in the mtDNA genotype can strongly influence the expressivity of autosomal gene mutations. Furthermore, the accumulation of somatic mtDNA mutations can augment the consequences of unfavorable mitochondrial-nuclear interactions.

Results

Transcriptional footprint of the Ant1-deficient heart

To clarify the molecular basis of the *Slc25a4* mutation-associated cardiomyopathy, we performed RNA sequencing on left ventricular myocardium of wild-type (WT) and *Ant1*-null mice. Changes in functionally annotated gene families were assessed by gene set enrichment analysis (GSEA). Significantly down-regulated pathways included extracellular matrix, intracellular signaling, chemotaxis, and mitochondrial antioxidant and fatty acid metabolism genes (Fig. 1A and S1). Up-regulated pathways included mitochondrial OXPHOS enzymes, canonical skeletal muscle proteins, and membrane-associated voltage-gated ion channels (Fig. 1B and S1).

The loss of structural extracellular components and the ectopic induction of skeletal muscle proteins in the myocardium are consistent with other forms of cardiomyopathy, as well as aging (Aronow et al., 2001; Houtkooper et al., 2011). The fibrotic alterations and cardiac remodeling from hypertrophic to dilated cardiomyopathy are also consistent with the observed pathology of the *Ant1*-null mouse (Burke et al., 2016; Graham et al., 1997; Narula et al., 2011).

The induction of OXPHOS components is particularly noteworthy, with complex I (NADH-ubiquinone/plastoquinone oxidoreductase) genes being among the most strongly up-regulated gene family in the *Ant1*-null heart (Fig. 1B). While the average change of all nDNA-coded OXPHOS polypeptide genes was slightly downregulated (Fig. 1C), the mtDNA-coded OXPHOS complex I subunits were strongly induced (Fig. 1D & E). The preferential upregulation of mtDNA complex I genes may represent a compensatory response to a partial impairment of complex I by the *Ant1* mutation.

nDNA-mtDNA genetic combinations and their effects on lifespan

Given the alterations in complex I expression of the *Ant1* mutation, we investigated the effects of combining the *Ant1* mutation with mtDNA mutations that resulted in partial defects in complex I, $ND6^{P25L}$, versus complex IV, COI^{V421A}. *Ant1* wild type (WT, $Ant1^{+/+}$)

and *Ant1* null (*Ant1$^{-/-}$*) mice were crossed with mice harboring normal, *ND6^{P25L}*, or *COI^{V421A}* mtDNAs. This resulted in six nDNA-mtDNA combinations: WT nDNA & WT mtDNA (WT); WT nDNA & *ND6^{P25L}* mtDNA (ND6); WT nDNA & *COI^{V421A}* mtDNA (COI); *ANT1$^{-/-}$* & WT mtDNA (ANT1); *ANT1$^{-/-}$* & *ND6^{P25L}* mtDNA (ANT1 ND6); and *ANT1$^{-/-}$* & *COI^{V421A}* mtDNA (ANT1 COI). In all cases, the nDNA background was derived from C57BL/6J into which the wild-type *Nnt* allele was reintroduced (C57Bl6/JEiJ) (Navarro et al., 2012).

In isolation, the *Ant1$^{-/-}$, ND6^{P25L}*, and *COI^{V421A}* mutations had a modest effect on mouse longevity relative to WT: the *COI^{V421A}* variant reduced lifespan by 9%, the *ND6^{P25L}* variant by 16%, and the *Ant1$^{-/-}$* by 22%. Combining the *Ant1$^{-/-}$* with the *COI^{V421A}* variant had minimal effect on the *Ant1$^{-/-}$* lifespan, but combining the *Ant1$^{-/-}$* with *ND6^{P25L}* reduced the lifespan by 49%, more than twice that of the *Ant1$^{-/-}$* alone (Fig. 2A). Therefore, combining *Ant1$^{-/-}$* with the *ND6^{P25L}* variant was significantly more deleterious than combining *Ant1$^{-/-}$* with *COI^{V421A}*.

The ANT1 and ANT1 ND6 mice exhibited morphological features of premature aging starting with kyphosis at six months (Fig. 2B), but COI, ND6, and ANT1 COI were indistinguishable from WT (not shown). By 15 months ANT1 and ANT1 ND6 mice had pronounced kyphosis, grey hair, and alopecia, while ANT1 COI mice appeared less effected (Fig. 2B). Basal motor activity levels of the ND6, ANT1, ANT1 COI, and ANT1 ND6 mice were significantly reduced in young mice, but COI mice were again indistinguishable from WT (Fig. 2C).

To assess the effects of nDNA-mtDNA interaction on metabolic robustness, core body temperature was first determined in mice housed at 22°C, which is ~10°C lower than their thermoneutral zone. This mild stress demands a ~60% increase in metabolic rate to maintain thermoregulation relative to thermoneutral temperature (Cannon and Nedergaard, 2011). WT, COI and ND6 mice maintained their core body temperature at

this standard housing condition. However, the core body temperatures of ANT1, ANT1 COI and ANT1 ND6 mice were reduced by an average of ~1.3° C relative to WT (Fig. 2D). This difference was not a product of weight, as the body weights of these mice were indistinguishable (Fig. S2). The metabolic stress was then increased by lowering the temperature to 4°C for six hours. The WT, COI and ND6 mice experienced a 1 to 2°C decline in core body temperature, while the ANT1 and ANT1 ND6 mice lost ~ 3°C in core body temperature (Fig. 2D). Surprisingly, the ANT1 COI strain maintained the same core body temperature in these extreme conditions as at 22°C ($\Delta 0.31 \pm 0.07$°C in ANT1 COI). Hence, the *Ant1* mutation has the greatest impact on thermal regulation in mild conditions, which the mtDNA *ND6*^{P25L} sustains, but the *Ant1* mutation effect is ameliorated by the mtDNA *COI*^{V421A} variant under more extreme environmental stress.

mtDNA variation alters the expressivity of age-dependent cardiomyopathy

Since ANT1-deficient humans (Strauss et al., 2013) and mice (Narula et al., 2011), manifest age-related, progressive cardiomyopathy, we investigated the relative cardiac weight and morphology of the six nDNA-mtDNA mouse strains over their lifespans (Fig. 3A). The relative heart weight of WT mice increased 0.06 ± 0.008 mg per gram of body weight per month of age ($r^2 = 0.32$; $p < 0.0001$). The mtDNA *COI*^{V421A} variant did not perturb this trend ($p = 0.32$), while the *ND6*^{P25L} variant reduced the relative heart weight increase seen in WT mice by ~21% ($p = 0.0003$; Fig. 3A).

Deletion of *Ant1* significantly increased the rate and extent of the age-related cardiac hypertrophy (Fig. 3A). Again, the *CO1*^{V421A} variant did not affect this trend ($p = 0.18$ for ANT1 COI *vs.* ANT1). However, combination of *ND6*^{P25L} with *Ant1*$^{-/-}$ increased the rate of cardiac enlargement ~200% over that of the *Ant1*$^{-/-}$ hearts ($p = 0.003$). By 15 months, the hearts of the ANT1 ND6 mice had increased 6.5-fold due to hypertrophic dilation, as evident in longitudinal sections of mutant hearts (Fig. 3B).

To further delineate cardiac structural and functional differences conferred by each nDNA-mtDNA combination, we employed echocardiography (ECG) with M-mode and speckle-tracking in B-mode for strain analysis. Strain reflects the total deformation of the ventricular myocardium during a cardiac cycle as a percentage of its initial length. Speckle-tracking based strain analysis provides valuable information about intrinsic contractile function, allowing assessment of myocardial pathophysiology prior to overt cardiac dysfunction (Biering-Sorensen et al., 2017; Geyer et al., 2010). There were no detectable differences in mice harboring either the mtDNA COI^{V421A} or $ND6^{P25L}$ variant related to WT across all echocardiographic parameters examined with this highly sensitive technique (Table S2). The mtDNA variants only affected cardiac structure or function when the nDNA $Ant1$ defect was also present. Addition of COI^{V421A} to $Ant1^{-/-}$ decreased left ventricular posterior wall thickness at systole (PWTs), but had no functional consequences on the $Ant1^{-/-}$ heart. Conversely, addition of the $ND6^{P25L}$ adversely affected every ECG measure, leading to dramatic ventricular dilation and an 80% reduction in cardiac contractility in ANT1 ND6 mice (Fig. 3C; Table S2). Thus, the partial complex I defect associated with the mtDNA $ND6^{P25L}$ markedly increased the severity of the $Ant1^{-/-}$ cardiomyopathy, while the partial complex IV defect caused by mtDNA COI^{V421A} had no detectable effect.

Effects of nDNA-mtDNA variation on cardiac ultrastructure

Abnormal mitochondrial morphology is commonly found in primary mitochondrial diseases, as well as in idiopathic cardiomyopathies. To determine how these genetic defects could influence mitochondrial morphology within the heart, we performed ultrastructural analysis of the left ventricle. The results revealed highly disordered myofibrils in all but the WT and COI strains (Fig. 4A-F), altered mitochondrial morphology (Fig. 4A'-F'), and increased lipofuscin aggregates (Fig. 4G) in strains with the shortest lifespan. While the mtDNA variants alone did not significantly alter mitochondrial content,

loss of ANT1 led to a 60% increase in mitochondrial number per mm^2 (Fig. 4H) and ANT1

COI and ANT1 ND6 hearts had over twice the amount of mitochondria as WT hearts (Fig.

4H). ND6, ANT1, and ANT1 ND6 ventricles show increased mitochondrial fragmentation,

with the ANT1 ND6 mitochondria reduced to half the size of all other strains (Fig. 4I-J

and S3). Notably, the COI^{V421A} variant had the reverse effect, leading to significant

mitochondrial enlargement, which counterbalanced mitochondrial fragmentation in the

Ant1-null heart (p = 0.64 for ANT1 COI *vs*. WT; Fig. 4I and S3).

In-depth ultrastructural analysis revealed that the WT, COI, and ND6 strains have similar

intramitochondrial structure, while all of the $Ant1^{-/-}$ strains are highly abnormal. The most

common intramitochondrial abnormalities were electron dense inclusions, hypodense

compartments, and cristae malformations (Fig. 4K-O, Fig. S4). Cristae morphology regulates

mitochondrial functions that are crucial for cardiac homeostasis, such as respiratory

efficiency, Ca^{++} buffering, ROS release, and apoptotic signaling (Cogliati et al., 2016).

Accordingly, the strains with the most severe dilated cardiomyopathy (ANT, ANT COI, and

ANT ND6) had the highest percentage of mitochondria with irregular cristae morphology

(i.e., reticular, partitioning, circular, concentric, and paracrystalline structures; Fig. 4L-O and

S4). The incidence of abnormal cristae was consistently higher in the ANT1 ND6

mitochondria than the ANT1 COI mitochondria. Thus, again, the combination of the $Ant1^{-/-}$

with mtDNA $ND6^{P25L}$ was more deleterious than the combination of $Ant1^{-/-}$ with mtDNA

COI^{V421A}.

Functional OXPHOS consequences of Ant1 and mtDNA mutations

To evaluate the biochemical differences between the single gene mutant strains

(ANT1, COI, and ND6) and the combination strains (ANT1 COI and ANT1 ND6), we

analyzed the activity and structural assembly of heart OXPHOS complexes I, IV and V.

Assaying the complex I, rotenone-sensitive, NADH:quinone oxidoreductase (NQR)

specific activity of 6 mo. old mice revealed that the complex I specific activity of the

$ND6^{P25L}$ mutant is reduced by 58% (Fig. 5A). Combination of the $Ant1^{-/-}$ with the $ND6^{P25L}$

mutant (ANT1 ND6) reduced the activity an additional 10%. At 18 months, the complex I

NQR activity in the ANT1 heart was reduced to the same low level as ND6, and their

combination (ANT1 ND6) reduced the heart complex I NQR activity an additional ~50%

(Fig. 5A). In contrast, complex I NQR activity in the COI mice remained normal at both 6

and 18 months, and complex I activity in the ANT1 COI heart was higher than that of the

ND6, ANT1, or ANT1 ND6 at 18 mo. (Fig. 5A), suggesting that the COI^{V421A} mtDNA

variant partially compensates for the $Ant1^{-/-}$ complex I defect.

To determine if the decline in NQR activity could be attributed to a decreased

amount of complex I, we measured the diaphorase activity of holoenzyme complex I

(Fig. 5B). While $ND6^{P25L}$ decreased the NQR specific activity of complex I by half, this

variant did not affect the actual amount of the holoenzyme (Fig. 5B). Surprisingly, $Ant1^{-/-}$

reduced holoenzyme levels by ~51% in 6 month-old hearts without affecting NQR

specific activity. The decreased amount of assembled complex I in ANT1 hearts was

confirmed by analysis of the complex I holoezyme with blue-native gel electrophoresis

(Fig. 5C). Both age and genotype significantly influenced complex I content, accounting

for 42% and 34% of the total variance, respectively, but age was the dominant factor (p

< 0.0001; two-way ANOVA for Age x Genotype). The $Ant1$ mutation appears to be the

major genetic influence on complex I amount, as all of the $Ant1$-deficient strains have

about half the holoenzyme levels of the respective $Ant1^{+/+}$ strains at each time point. The

reason for the reduced cardiac complex I content associated with the $Ant1$ mutation and

age is unknown, but could be the result of decreased stability during mitochondrial

isolation, an assembly defect, increased degradation, or a combination of these factors.

Complex IV (COX) activity was measured by cytochrome c oxidation in myocardial

homogenates, and the specific activity normalized to citrate synthase (CS) activity (Fig.

5D-E). CS activity was increased by 25% in $Ant1$-deficient myocardium, but decreased

by the addition of $ND6^{P25L}$ (Fig. 5D). COX/CS activity was reduced to 39% of control by the mtDNA COI^{V421A} mutation, but the additional loss of $Ant1$ (ANT1 COI) had no appreciable effect. $Ant1^{-/-}$, $ND6^{P25L}$, or their combination, had no effect on the COX/CS activity up to 18 months of age.

Since the $Ant1$-null hearts have abnormal cristae structure and complex V (F_1F_0 ATPase) dimerization is necessary for proper cristae formation (Davies et al., 2012; Paumard et al., 2002; Strauss et al., 2008), the structure and supercomplex assembly of complex V was also examined. To determine if loss of $Ant1$ altered the dimer equilibrium of the F_1F_0 ATPase, we analyzed high-molecular weight F_1F_0-ATPase oligomers by clear-native gel electrophoresis using mild solubilizing conditions (3% digitonin) (Wittig et al., 2010). $Ant1$-deficiency drastically reduced F_1F_0-ATPase dimers and oligomers (Fig. 5F). Analysis using the more stringent detergent (2.5% dodecylmaltoside, DDM) revealed the ATP synthase holocomplex monomers (V) are also labile and give rise to subcomplexes V^*a and V^*b (Fig. S5), though all fragments retained ATP hydrolysis activity. The F_1F_0 ATPase subcomplexes observed in the $Ant1$-null heart mitochondria resemble those reported in mtDNA depleted (p^0) cells (Wittig et al., 2010) and in cells harboring $ATP6$ and $ATP8$ mutations (Carrozzo et al., 2006; Mourier et al., 2014; van der Westhuizen et al., 2010) suggesting that loss of $Ant1$ impairs the assembly of the F_0 component of the ATP synthase.

Mitochondrial Respiration, ROS Production, and mtPTP Activation

To determine how these genetic defects alter mitochondrial physiology, we isolated cardiac mitochondria from 6 and 18 month-old animals. Inactivation of $Ant1$ increased the cardiac mitochondrial membrane potential ~25-30% in young ANT1, ANT1 COI, and ANT1 ND6 hearts relative to WT, COI, and ND6 hearts (Fig. 6A), possibly caused by the subassembled ATP synthase (complex V) (Mourier et al., 2014), or its diminished activity due to limited availability of matrix ADP (Graham et al., 1997) .

Oxygen consumption was measured in cardiac mitochondria respiring on the complex I, NADH-linked, substrates glutamate and malate (GM). Heart mitochondrial respiration rates in the *LEAK* (*L*) state (in the absence of ADP or uncoupler) were suppressed by the *COI*[V421A] mutation (Fig. 6B). In the presence of ADP, the *ND6*[P25L] mutation impaired respiration by ~20% (Fig. 6C). Thus, the mtDNA mutations affect different aspects of mitochondrial function. Interestingly, ANT1-deficiency did not impair ADP stimulated respiration in young animals (Fig. 6C), possibly due to ANT2-facilitated ADP import into the mitochondria (Brand et al., 2005).

To determine the importance of the ATP synthase on state III (ADP-stimulated; *P*) respiration, we treated mitochondria respiring on GM and ADP with the F_1F_0ATP synthase inhibitor oligomycin. Oligomycin reduced the state III respiration rate of WT, COI, and ND6 mitochondria 80%, consistent with mitochondrial respiration being predominantly coupled to the ATP synthase through use of the proton gradient to synthesize ATP (Fig. 6D). The residual 20% oligomycin resistant respiration of WT, COI and ND6 heart mitochondria likely reflects the non-specific proton leak. Conversely, oligomycin only reduced *Ant1*-null mitochondrial respiration by 50-60% (Fig. 6D). The diminished effect of oligomycin may be due to the limited mitochondrial ADP import due to the loss of ANT1 plus impaired ATP synthase function and assembly (Mourier et al., 2014). The remaining 40-50% of oligomycin sensitive respiration may reflect ADP import into the mitochondria by ANT2.

To determine if heart mitochondria with different nDNA-mtDNA genetic combinations display altered mitochondrial ROS production, we analyzed mitochondrial H_2O_2 emission using the Amplex Red assay (Fig. 6E). When mitochondria were respiring on NADH-linked substrates (GM), H_2O_2 emission rates were 18-48% increased in mitochondrial harboring the *COI*[V421A] mutation, as well as all *Ant1*-deficient mitochondria (Fig. 6E, GM). Treatment with rotenone (R), which binds to the complex I CoQ binding site downstream

of the site of NADH reduction and enhances ROS production via forward electron transfer (Murphy, 2009) reduced COI^{V421A} ROS production but increased $ND6^{P25L}$ ROS production. When the complex II substrate, succinate, was added as the electron donor and the membrane potential maximized by blocking the ATP synthase with oligomycin, the electrons are driven backward from CoQ into complex I resulting in ROS production by reverse electron transfer (RET) (Brand, 2010; Chouchani et al., 2014; Murphy, 2009). In this case, ROS production from the ND6 and ANT1 ND6 heart mitochondria was abolished (Fig. 6E, Succ + Oligo), consistent with our previous studies showing that $ND6^{P25L}$ blocks ROS production by RET in liver and brain (Lin et al., 2012). By contrast, WT, ANT1 and COI showed robust ROS production by RET. Hence, WT, COI, ANT1, and ANT1 COI mitochondria generate ROS by both forward and reverse electron transfer, while ND6 only generates ROS by forward electron flux. Since the mtDNA $ND6^{P25L}$ mutation blocks RET, yet the $ND6^{P25L}$ mitochondria generate more comparable ROS to ANT1 and COI mitochondria, it follows that the ND6 mitochondria must generate more ROS by forward electron flux through complex I than the other mutations (Fig. 6E, GM+R).

Excessive mitochondrial ROS production via forward electron flux induces ryanodine receptor-dependent Ca^{++} release and sensitizes the mtPTP. This causes impaired cardiac contractility and increased mitochondrial permeability transition (Zorov et al., 2000). Since ANT1 ND6 hearts have the most diminished contractility and highest ROS production by forward electron flux, we hypothesized that their mitochondria would also be most susceptible to permeability transition. To assess this possibility, we quantified the effect of each nDNA-mtDNA combination on the sensitivity of ventricular mitochondria to Ca^{++}-mediated permeability transition. Loss of ANT1 alone did not increase the Ca^{++} sensitivity of the mtPTP in heart mitochondria (Fig. 6F). However, the

combination of $Ant1^{-/-}$ and $ND6^{P25L}$ did sensitize the mtPTP to Ca^{++} activation, rendering ANT1 ND6 hearts more prone to permeability transition (Fig. 6F-G).

mtDNA somatic mutations and apoptosis in cardiac aging

Since the ANT1 and COI and ND6 alterations are present at birth, the progression of the cardiomyopathy of the ANT1 ND6 mutant hearts implies the presence of an additional age-related mitochondrial factor. To determine if this additional factor was associated with the accumulation of somatic mtDNA mutations (Vermulst et al., 2008b), we analyzed the relative levels of deleted mtDNAs in ventricular tissue from the six nDNA-mtDNA combinations using long extension PCR (LX-PCR) (Fig. 7A-B) and random mutation capture quantitative PCR (Fig. S7A)(Vermulst et al., 2007; Vermulst et al., 2008a; Vermulst et al., 2008b). mtDNA deletion load at 12-15 mo. was highest in strains with the most severe cardiomyopathy and mortality (Fig. S7B-C), with ANT1 ND6 hearts accumulating the most mtDNA deletions (Fig. 7B).

Increased mtDNA deletions and mtPTP sensitization induce caspase activation and death of cardiomyocytes, thereby accelerating the progression of hypertrophic cardiomyopathy (Dai et al., 2010; Mott et al., 2004). Accordingly, caspase 3/7 activities were highest in the ANT1 ND6 myocardium (Fig. 7C). Hence, the increased somatic mtDNA mutation load of the combined $Ant1^{-/-}$ and mtDNA $ND6^{P25L}$ variants in the hearts may explain the rapid rise in cardiac size and progression to dilated cardiomyopathy in the ANT1 ND6 mice.

Discussion

mtDNA variants have been associated with variable expressivity of contractile gene mutations causing hypertrophic cardiomyopathy and heart failure (Arbustini et al., 1998b). Furthermore, mtDNA haplogroup variants correlate with the severity of *ANT1-*induced cardiomyopathy (Strauss et al., 2013). Still, whether mtDNA determines the

variable phenotypic expression of autosomal gene mutations and how such mitochondrial-nuclear interactions contribute to cardiovascular disease remains unknown.

To confirm that mtDNA variants can modulate the phenotypic manifestation of nDNA gene mutations, we analyzed the cardiac function and mitochondrial physiology of mice sharing the nuclear *Ant1* null mutation (Graham et al., 1997; Narula et al., 2011), but with different mtDNAs (WT, *ND6*^{P25L} or *COI*^{V421A}). Importantly, neither mtDNA *ND6*^{P25L} nor *COI*^{V421A} variant alone had an appreciable effect on cardiac physiology. The *COI*^{V421A} variant also had minimal effect on the *Ant1*$^{-/-}$ cardiac pathophysiology. By contrast, the mtDNA *ND6*^{P25L} variant has a strikingly negative influence on the *Ant1*$^{-/-}$ phenotype, resulting in a rapidly progressive, and ultimately fatal, dilated cardiomyopathy. The markedly different effects of the *COI*^{V421A} and *ND6*^{P25L} mtDNA OXPHOS variants on *Ant1*$^{-/-}$-induced cardiomyopathy is proof of principle that mtDNA can exert modifier effects on the phenotypic expressivity of autosomal gene mutations.

Further evidence that nDNA-mtDNA interactions can determine the severity of cardiomyopathy is found in our concurrent discovery that the nDNA *Nnt* genotype exerts a marked modifier effect on the cardiac phenotype of the mtDNA *COI*^{V421A} variant. C57Bl/6J mice are homozygous for a truncated *Nnt* allele (*Nnt*$^{/-}$), which itself causes no overt cardiac defects in mice (Freeman et al., 2006; Huang et al., 2006; Toye et al., 2005). As we reported previously, the mtDNA *COI*^{V421A} variant on the C57Bl/6J *Nnt*$^{/-}$ background causes hypertrophic cardiomyopathy (Fan et al., 2008). However, when transferred onto the C57Bl/6JEiJ *Nnt*$^{+/+}$ nuclear background, the mtDNA *COI*^{V421A} variant gave virtually wild type cardiac function (Fig. 3C). Hence, the *COI*^{V421A} acts synergistically with the *Nnt*$^{/-}$ null mutation while the *ND6*^{P25L} mutation acts synergistically with the *Ant1*$^{-/-}$ null mutation.

Having established that mitochondrial-nuclear interactions do modulate both mtDNA and nDNA phenotypic expression, we employed our unique mitochondrial mouse models ($Ant1^{-/-}$, COI^{V421A}, and $ND6^{P25L}$) to investigate the pathophysiological basis of this relationship. Our analysis revealed four major mechanisms by which the mtDNA variation modulates $Ant1$ expressivity: OXPHOS complex I function, differential ROS production, mPTP sensitivity, and somatic mtDNA mutation rate. First, $Ant1^{-/-}$ and $ND6^{P25L}$ both perturb complex I, with $Ant1^{-/-}$ reducing the amount of structurally assembled complex I while the $ND6^{P25L}$ variant reduces the complex I specific activity. Second, the $ND6^{P25L}$ variant generates comparable total ROS production as $Ant1^{-/-}$ and the COI^{V421A} variant. However, the $ND6^{P25L}$ variant produces ROS by only forward electron transfer, as opposed to both forward and reverse electron flux for the $Ant1^{-/-}$ and COI^{V421A} variants. Since in normoxic conditions the high energetic load of the heart would require high ATP production, forward electron transfer must be favored. So the mtDNA $ND6^{P25L}$ mutation must generate more forward electron flow ROS than the mtDNA COI^{V421A} mutation. Moreover, reverse electron flow (RET) induces mitochondrial hormesis, which is protective of age-related disease and extends lifespan (Scialo et al., 2016). Since $ND6^{P25L}$ blocks RET, this cytoprotective effect would be lost for the mtDNA $ND6^{P25L}$ but not for the COI^{V421A}. Third, the $Ant1^{-/-}$ and $ND6^{P25L}$ combination sensitizes cardiac mitochondria to Ca^{++}-induced mtPTP permeability transition while the $Ant1^{-/-}$ and COI^{V421A} combination does not. This is consistent with increased deleterious ROS production and defective cardiac contractility in the $Ant1^{-/-}$ $ND6^{P25L}$ genotype (Zorov et al., 2000). Finally, the $Ant1^{-/-}$ $ND6^{P25L}$ combination results in a higher mtDNA somatic mutation rate than the $Ant1^{-/-}$ COI^{V421A}, which may amplify the inherited mitochondrial defects over time and accelerate the progression of cardiomyopathy (Vermulst et al., 2007; Vermulst et al., 2008b).

The distinct alterations in mitochondrial ultrastructure conferred by the mtDNA variants are consistent with their respective biochemical and molecular consequences on *Ant1* expressivity. The effect of mtDNA *COI*^{V421A} and *ND6*^{P25L} on mitochondrial morphology is diametrically opposed, with *COI*^{V421A} increasing mitochondrial size, and *ND6*^{P25L} causing severe mitochondrial fragmentation. The combination of *Ant1*$^{-/-}$ and *ND6*^{P25L} further reduces mitochondrial size and increases the number of cristae partitions implying early stage fission. Mitochondrial fragmentation not only induces more ROS production and mtDNA damage (Yu et al., 2008), it also impairs the mixing of multiple mtDNAs within the same mitochondrion, thereby blocking the benefits of inter-mtDNA complementation (Chen et al., 2010). Accordingly, increased *de novo* somatic mtDNA mutations due to *Ant1*$^{-/-}$ (Fig. 7A-B, Fig. S7A) would be more deleterious when combined with *ND6*^{P25L} than *COI*^{V421A}. Indeed, the apparent mitochondrial hyperfusion by *COI*^{V421A} normalizes *Ant1*$^{-/-}$-induced fragmentation (Fig. 4I, Fig. S3) which partially protects against mtDNA deletion accumulation and caspase activation (Fig, 7B-C) thus preventing the decline in *Ant1*$^{-/-}$-mitochondrial function with age (Fig. S6).

In conclusion, we have shown that the severity of the cardiomyopathy caused by a nuclear gene mutation can be directly modulated by the presence of otherwise sub-pathogenic mtDNA variants. This was true both for the differential effects of the *ND6*^{P25L} and *COI*^{V421A} mtDNA variants on the *Ant1*$^{-/-}$ mutation as well as for the *COI*^{V421A} versus WT mtDNA variants on the *Nnt*$^{-/-}$ mutation. These results demonstrate that nDNA-mtDNA interactions can play a critical role in modulating the phenotyps of nDNA gene mutations.

Methods

Mouse Genetics

All mice were maintained on the C57Bl/6JEiJ background, which was derived from the Jackson Laboratory C56Bl/6J line into which the wild-type (WT) nicotinamide nucleotide transhydrogenase (*Nnt*) gene was reintroduced (Navarro et al., 2012), herein designated as WT. These mice were compared to mice harboring the mtDNA NADH dehydrogenase subunit 6 gene (*ND6*) nt 13997G>A P25L or cytochrome c oxidase subunit I gene (*COI*) nt 6598T>C V421 mutations generated via the female embryonic stem (ES) cell fusion method (Fan et al., 2008; Lin et al., 2012). The phenotypes of these mtDNA variants, as well as the adenine nucleotide translocator isoform 1 (*Ant1*)-null gene (Graham et al., 1997; Narula et al., 2011), were previously reported on the C56Bl/6J *Nnt*$^{-/-}$ strain. We transferred the *Ant1*$^{-/-}$, *ND6*^{P25L}, and *COI*^{V421A} mutations in to the C57Bl/6JEiJ strain by repeated backcrosses to remove the confounding influence of the nuclear modifier, *Nnt* (Huang et al., 2006; Kim et al., 2010). The C57Bl/6JEiJ *Ant1*$^{-/-}$ males were then crossed with female C57Bl/6JEiJ *ND6*^{P25L} or *COI*^{V421A} to attain C57Bl/6JEiJ *Ant1*$^{-/-}$ *ND6*^{P25L} and C57Bl/6JEiJ nDNA-*Ant1*$^{-/-}$ *COI*^{V421A} mice. The WT and *Ant1*$^{-/-}$ mice were maintained by brother-sister matings. The mtDNA *ND6*^{P25L} and *COI*^{V421A} mutant mice were maintained by crossing female mtDNA mutant mice with WT males. The *Ant1*$^{-/-}$ *ND6*^{P25L} and *Ant1*$^{-/-}$ *COI*^{V421A} mutant mice were maintained by crossing the Ant1$^{-/-}$ *ND6*^{P25L} and Ant1$^{-/-}$ *COI*^{V421A} females with *Ant1*$^{-/-}$ males.

Mouse maintenance and longevity

All experimental procedures involving mice were conducted in accordance to approved Institutional Animal Care and Use Committee (IACUC) protocols at the Children's Hospital of Philadelphia. To eliminate confounding effects of estrogen on mitochondrial physiology, only male mice were considered in our analyses (Duckles et al., 2006; Eichner and Giguere, 2011). Male mice were pooled at weaning to attain 3 – 5,

genotype-, sex- and age-matched mice per cage with *ad libitum* access to food and water, on a 13:11 light:dark cycle. A minimum of 3 subjects per strain were used for all experiments, except assessment of respiratory complex I assembly by blue-native electrophoresis (n = 2). Additional subjects were included, as noted, based on the availability of age- and strain- matched mice and nature of the assay (Lin et al., 2012; Narula et al., 2011). During sample preparation, subjects were randomly numbered to blind the experimenter for subsequent tests and analysis. The effect of specific mitochondrial genetic variation on longevity was determined by Kaplan–Meier survival curves constructed from the known date of birth and death of at least one hundred mice per genotype. Apart from cage changes and daily health checks, these mice were left undisturbed. When mice were determined moribund by the veterinary staff, they were humanely euthanized and the date of death recorded. Differences between groups were evaluated using the log-rank (Mantel-Cox) test (GraphPad, La Jolla, CA, USA).

RNA-sequencing and bioinformatics

Total RNA was extracted in Trizol with a motorized pestle from 30-60 mg of left myocardium (n = 4) and processed with the PureLink RNA-Easy kit (Life technologies #12183018A), and affinity-depleted of ribosomal RNA (rRNA) with magnetic bead RiboMinus™ Eukaryote System v2 (Life technologies # A15026). PolyA enrichment was avoided to maximize recovery of mtDNA-encoded transcripts. Purified RNA was quantified and quality checked with RNA 6000 Pico chip (Agilent #5067-1513) on Agilent Bioanalizer 2100, and spiked with the ERCC RNA Spike-In Mix (4456740). Library preparation was performed from 800 ng of rRNA-depleted RNA and processed with the Ion Total RNA-Seq Kit v2 (Life technologies #4475936) and multiplexed-sequenced with Ion PI Sequencing 200 Kit v2 chemistry (Life Techologies #4485149) on the Ion Proton platform. Two samples were pooled per chip, yielding on average > 25 million reads per sample, and an average read length of ~80 bp. After trimming, transcript counts were

generated by a STAR alignment to the reference mouse genome, mapping to a total of 14,642 annotated genes, and normalized using ERCC spike-ins counts. Differential expression, fold change, and statistical significance for each gene was established using the DESeq Bioconductor package in R. DESeq. Data was subsequently analyzed for individual genes of interest, or using DAVID (Database for Annotation, Visualization and Integrated Discovery v6.7) to derive functional significance of up- and down-regulated pathways of interest.

Data Management

Raw sequence files and associated metadata have been deposited in NCBI SRA (SUB2425516). Reproducible code for generating the values presented in this paper is located at https://github.com/chop-dbhi/mcmanus_ant1.

Cardiac Size and Histopathology

Hearts were excised, weighed, and fixed in 4% paraformaldehyde for at least 48 h. Relative heart weight was determined by the ratio of heart to body weight over the lifespan of each strain (n = 65 - 111). Longitudinal sections of paraffin embedded tissues were sliced and stained with hematoxylin and eosin stain (H & E; n = 3).

Calorimetry

Energy expenditure was assessed using indirect calorimetry (Oxymax; Columbus Instruments). Mice were singly housed with water and food ad libitum (n = 6). After a 3-day acclimation period, oxygen consumption and carbon dioxide production were measured over 30 h using an air flow of 600 mL/min at 22°C. For the cold stress challenge, mice were placed in 4°C for 6 h. Core body temperature was measured using a rectal probe (Harvard Apparatus).

Speckle tracking echocardiography of left ventricular mechanics

Images were obtained using the Vevo2100 equipped with a MS550D transducer (Visual Sonics, Toronto, ON, Canada). The mice were lightly anaesthetized using 1.5%

isofluorane mixed with 100% O_2 during the time of imaging. Electrocardiography leads were applied to monitor heart rate and trigger echo image acquisitions. The images were obtained from the B-mode long-axis view and the M-mode of the parasternal short-axis view. Speckle tracking echocardiography (STE) was performed as a sensitive indicator of myocardial contractility using Vevostrain software (Visual Sonics, Toronto, ON, Canada) incorporated into the Vevo2100 from the movies acquired from the B-mode long-axis view. The tracking quality was visually inspected, and the tracing was confirmed as acceptable when the traced line moved along with the moving heart image for at least three cardiac cycles. These cardiac cycles were used for the analysis. . Strain analysis was performed using speckle tracking algorithms applied on high-frequency ultrasound images. Parasternal long-axis view provided longitudinal strain, whereas, parasternal short axis view was used for assessing circumferential strain. M-mode images at mid-LV were used to determine left ventricular internal dimension at end-diastole (LVIDd) and LV dimension internal dimension at end-systole (LVIDs). The LV ejection fraction (EF) was calculated. Interventricular septum (IVS) wall thickness and left ventricular posterior wall (LVPW) thickness were obtained (n = 10 – 34).

Mitochondrial morphology

Thin slices of left ventricular myocardium were excised from 6 month old animals of each genotype and immediately immersed in fixation buffer containing 2% glutaraldehyde and 0.1 M cacodylate (pH 7.4) (Picard et al., 2015). Samples were post-fixed in 2.0% osmium tetroxide for 1 h at room temperature and rinsed in distilled H_2O before in-bloc staining with 2% uranyl acetate. After dehydration through a graded ethanol series, each sample was embedded in EMbed-812 (Electron Microscopy Sciences, Fort Washington, PA). Cardiomyocyte orientation and quality were first checked in 1 μm thick sections stained with 1% toluidine blue. Thin sections (90 μm) were then mounted on filmed copper grids and stained with uranyl acetate and lead

citrate and examined on a JEOL 1010 electron microscope fitted with a Hamamatsu digital camera and AMT Advantage image capture software. Myocardial mitochondria were manually traced from at least 8 calibrated images per subject at x12,000 indirect magnification using Image J (National Institutes of Health, Bethesda, MD). To produce frequency distributions of morphological parameters, the area of each mitochondrion was assigned to one of twenty bins of equal size. Lipofuscin granules were counted per image and normalized to the mean of WT. Abnormal mitochondria were counted and expressed as percent of total mitochondria per image. The most common types of cristae defects found across all strains were manually quantified. Statistical significance was evaluated based on 95% confidence interval (C.I.) of the mean.

Mitochondrial Isolation

Mitochondria were isolated from murine hearts (Palmer et al., 1977). The entire procedure was performed on ice or in a cold room ($4^{o}C$). Ventricular tissue was excised, blotted, weighed, rinsed and diced in a small beaker containing 2 mL of ice-cold organ preservation solution (BIOPS) comprised of 2.77 mM CaK_2 EGTA buffer, 7.23 mM K_2 EGTA buffer, 0.1 µM free calcium, 20 mM imidazole, 20 mM taurine, 50 mM 2-(N-morpholino) ethanesulfonic acid hydrate (MES), 0.5 mM dithiothreitol, 6.56 mM $MgCl_2 \cdot 6H_2O$, 5.77 mM ATP, and 15 mM phosphocreatine (pH 7.1). The buffer was decanted, and tissue digested in 0.015% trypsin for 10 min. The protease was neutralized by 5x dilution in isolation buffer (50 mM MOPS, 100 mM KCl, 1 mM EGTA, 5 mM $MgSO_4$, 1mM ATP) containing 10 mg/ml fatty acid-free BSA. The tissue was electrically homogenized using a Eurostar Power B (1100 rpm x 7-8 strokes) and mitochondria isolated by differential centrifugation. The final pellet was resuspended in the appropriate experimental buffer.

Complex I Activity

Complex I NADH-ubiquinone reductase (NQR) activity (Ji et al., 2014) was assayed using 25 µg/ml of isolated mitochondria using the complex I assay buffer (250 mM sucrose, 10 mM Hepes, 0.2 mM EDTA, 2.5 mM $MgCl_2$, pH 7.2) containing 40 µg/ mL alamethicin to permeabilize the mitochondria inner membrane. After one minute, the reaction was started by addition of 100 µM coenzyme Q_1, and 200 µM NADH. NADH oxidation was monitored at 340 nm using a Cary300 dual-beam spectrophotometer at 30 °C, and rotenone sensitive activity calculated. NQR activity was determined by subtracting the basal (no substrate) and the rotenone (4 µM) insensitive rates from the NADH:CoQ_1 rate. The results are shown as nmol NADH mg^{-1} min^{-1} using the extinction coefficient of NADH at 340 nm (6.22 mM^{-1} cm^{-1}). The assay was performed in 3 independent trials (n = 3 - 7).

The amount of assembled complex I was estimated by assaying diaphorase-type activity from complex I immunocaptured from isolated heart mitochondria (10 µg/ml) (Abcam; ab109721). The assay was performed in 2 independent trials (n = 3 - 6).

Native gel electrophoresis and immunodetection

Mitochondrial respiratory complexes were separated by native electrophoresis for analysis of complex I assembly (Yadava et al., 2002). Fresh mitochondrial pellets equivalent to 400 µg of protein were solubilized with 800 µg of dodecyl-β-D-maltoside (DDM; Sigma) in 5 mM 6-aminohexanoic acid, 50 mM imidazole-HCl (pH 7.0) and 10% glycerol. Coomassie Brilliant Blue G-250 (Serva) was added to the solubilized samples at a dye/detergent ratio of 1:5 (w/w). The samples were loaded on a 4-13% acrylamide gradient gel and electrophoresed overnight. Proteins were transferred to PVDF membranes from the native gels and western blotting performed using standard transfer conditions for 3 h. The blots were de-stained by washing with 100% methanol and then probed with NDUFA1 antisera to determine complex I assembly (n = 2; antibody provided by Scheffler IE; validated in (Yadava et al., 2002)).

The assembly and oligomerization state of F_1F_o ATPase were determined using clear native electrophoresis (CNE) (Wittig et al., 2007). To quantify the holo-complex V (V_m) stability, mitochondrial protein was solubilized on ice for 15 min with 2.5% DDM. The samples were then centrifuged for 30 min at 25000 g, 4°C, and equal mitochondrial protein loaded on CNE gels. The complexes were electrophoresed overnight at 100 – 120 mV; the gel incubated in 35 mM Tris (0.42%), 270 mM Glycine (2.02%), pH 8.3 for 2h; and washed in the same buffer supplemented with 14 mM $MgSO_4$, 0.2% $Pb(NO_3)_2$, and 8 mM ATP until the white lead phosphate precipitated. The reaction was stopped with 50% methanol, and the gel imaged. Western blots of duplicate gels were probed with a anti-mouse VDAC monoclonal antibody as a loading control (Abcam; ab14734). The assay was performed in 4 independent trials (n = 4).

Cytochrome-c oxidase and citrate synthase activity

Frozen samples from the left ventricular myocardium were thawed on ice and approximately 10 mg of each was diced and homogenized with a Teflon pestle at 1:30 (w/v) in 50 mM triethanolamine with 1 mM EDTA (pH 7.4). The samples were solubilized in potassium phosphate buffer and 0.1% (w/v) n-dodecylmaltoside (pH 7.5). The reaction was started by the addition of 0.1 mM reduced ferrocytochrome *c* (0.1 mM) and the initial rate of oxidation determined by following the decrease in absorbance at 550 nm in a 96-well plate at 30°C (Capaldi et al., 1995). To control for differences in myocardial mitochondrial content, citrate synthase (CS) activity was determined from the same tissue homogenates (Mofarrahi et al., 2013). The samples were diluted 1:26 in CS buffer (100 mM Tris, 0.2 mM acetylCoA, 0.2 mM 5,5-dithio-bis-2-nitrobenzoic acid (DTNB), 70 µM oxaloacetate) and the change in absorbance of DTNB was measured at 412 nm. Parallel samples in buffer lacking oxaloacetate were included as negative controls to ensure specificity of the reaction. The molar extinction coefficients used were

29.5 L mol^{-1} cm^{-1} for ferrocytochrome *c* and 13.6 L mol^{-1} cm^{-1} for DTNB. Each assay was performed twice, n = 4 − 6.

Respiration

High-resolution respirometry of isolated mitochondria was performed in ice-cold mitochondrial respiration medium 5 (MiR05: 0.5 mM EGTA, 3 mM MgCl$_2$, 60 mM potassium lactobionate, 20 mM taurine, 10 mM KH$_2$PO4, 20 mM HEPES, 110 mM sucrose, and 1 g/L BSA essentially fatty acid free, adjusted to pH 7.1) at 25°C using the Oxygraph-2k (Oroboros, Innsbruck, Austria). Sequential oxygen consumption rates were determined in mitochondria respiring first on malate (2 mM) and glutamate (10 mM) (state II; *L = LEAK*), followed by addition of 2.5 mM ADP (state III; *P* state), then the addition of oligomycin (2 µg/mL) (state 4), and lastly addition of rotenone and antimycin A (residual oxygen consumption; ROX). The quality of the mitochondrial preparations was confirmed by the absence of a cytochrome *c* effect on oxygen consumption in the *P* state (data not shown). Respirometry experiments were conducted in pairs of over 18 independent experiments, n = 3.

Mitochondrial reactive oxygen species (mtROS) and membrane potential (MMP)

The rate of mtROS production was determined by monitoring the oxidation of the fluorogenic indicator Amplex Red by H$_2$O$_2$ in the presence of horseradish peroxidase as previously described (Lin et al., 2012). Mitochondria (0.05 mg/ml) were incubated in assay medium [125 mM KCl, 20 mM Hepes, 2 mM K$_2$HPO$_4$, 1 mM MgCl2, 0.1 mM EGTA, 0.025% BSA (pH 7.2) at 37 °C]. Glutamate and malate (5 mM each) were used to induce forward electron transfer. For reverse electron transfer experiments, 5 mM succinate and 1 µg/ml oligomycin were included. Amplex Red (1 µM) and 5 U·mL−1 horseradish peroxidase were added to initiate the reaction. Fluorescence was recorded at excitation 560 nm and emission 590 nm. Mitochondrial membrane potential (MMP) was assessed on 0.025 mg mitochondria using the potentiometric fluorescent dye

TMRM (100 nM) (535 nm excitation, 600 nm emission) while metabolizing the complex I substrates malate and glutamate. The results were normalized by comparison with a parallel experiment but with the FCCP (carbonyl cyanide-*4*-(trifluoromethoxy) phenylhydrazone) uncoupler added. Each sample was run in triplicate, n = 3, in two independent experiments, and results are shown as fold change from WT per condition.

Calcium retention capacity

The mitochondrial calcium retention capacity (CRC) of mitochondrial preparations (Tiepolo et al., 2009) was assessed by monitoring Ca^{++} uptake and release using the Ca^{++} indicator, Calcium Green-5N (1 mM; excitation, 505 nm; emission, 535 nm), monitored using a Fluoromax spectrofluorometer (Horiba; Kyoto Japan) equipped with magnetic stirring rod. The incubation medium contained 0.2 M sucrose, 10 mM Tris-MOPS, 5 mM glutamate-Tris, 2.5 mM malate-Tris, 1 mM. Final volume was 2 mL, pH 7.4, 25°C. All the experiments were started with the addition of 0.5 mg/ml mitochondria followed 1 min later by the indicated pulses of Ca^{++}. Each sample was run in duplicate. Traces are representative for the group (n = 3 - 4).

mtDNA deletion analysis

Whole genomic DNA was isolated from the ventricular myocardium using phenol-chloroform-isoamyl alcohol extraction and diluted to 2.5 ng/µl. mtDNA deletions were detected by amplification of a 12.8 kB mtDNA fragment using Accuprime Hi Fi (Invitrogen 12346068) and the following primer pairs: <u>ND2 Forward</u>: *5'CTGGAATTCAGCCTACTAGCAATTATCC-3'*; <u>12s Reverse</u>: *5'-TTTAGGTTTATGGCTAAGCATAGTGGGG- 3'*. The long template PCR products were equally loaded and run in 2 TBE (0.8%) gels and the number of bands per sample (n = 4 - 6) quantified by ImageJ.

To quantify the deletion burden at a particular site, the random mutation capture (RMC) assay was adapted to detect large deletions in the major arc between two 15-bp

direct repeats previously shown to be hotspots for mtDNA deletions (Vermulst et al., 2007; Vermulst et al., 2008a; Vermulst et al., 2008b). Briefly, mtDNA was first digested by Taq1 to remove WT mtDNA. The number of mtDNA molecules with a deletion were then determined using the following qPCR primers, spaced several kb apart, flanking multiple TaqI restriction sites: <u>Deletion Forward</u>: *5'-AGGCCACCACACTCCTATTG-3'*, position 8810-8829; <u>Deletion Reverse</u>: *5'-AATGCTAGGCGTTTGATTGG -3'*, position 13098-13117. The total number of mtDNA molecules per sample was determined using the following control primers that do not include a Taq1 site: <u>Control Forward</u>: *5'-TCGGCGTAAAACGTGTCAAC-3'*, position 350-369; <u>Control Reverse</u>: *5'-CCGCCAAGTCCTTTGAGTTT-3'* position 579-598. The ratio of deleted mtDNA molecules to total mtDNA molecules was used to determine the deletion frequency, and the results were normalized to WT. The assay was performed in two independent experiments, n = 3 - 5.

Caspase-3/7 Activity

To detect caspase-3/7 activity, mouse hearts were homogenized in hypotonic extraction buffer (25 mM HEPES [pH 7.5], 5 mM $MgCl_2$, 1 mM EGTA) on ice. The homogenates were cleared by centrifugation at 13,000 rpm for 15 minutes at 4°C. Protein concentrations were adjusted to 1 mg/ml, and an equal volume of 10 μg/ml added to the Caspase-Glo® Reagent (Promega G8091). The assays were incubated for one hour at room temperature before reading on a luminometer (SpectraMax Paradigm; Eugene, OR). n = 4, performed in two independent experiments.

Statistical Analysis

The data was quantified in Prism 6.0 (GraphPad, La Jolla, CA, USA), and the appropriate statistical analysis performed using one-way or two-way ANOVAs, corrected for multiple comparisons by the Sidak post hoc test, unless noted otherwise. The Brown-

Forsythe test was used to determine differences in standard deviations among groups, and the Geisser-Greenhouse correction applied for sphericity.

Figure Legends

Figure 1. ANT1-deficiency induces transcriptional changes associated with pathological remodeling of heart. Twenty-five most significantly down- (>2 fold, total = 459; **A**) and up-regulated (<0.4 fold, total = 363; **B**) functionally annotated gene categories in *Ant1*-null myocardium compared to WT. Searched categories include Gene Ontology (GO), Protein Information Resource (PIR), Sequence (Seq) Features, Kyoto Encyclopedia of Genes and Genomes (KEGG), InterPro protein sequence and analysis classification. Analysis performed using the Database for Annotation, Visualization and Integrated Discovery (DAVID, v6.7). (**C**) Fold change in mRNA transcripts from nDNA and (**D**) mtDNA OXPHOS genes by complex relative to WT. (**E**) Portion of differentially expressed RNA transcripts from mtDNA. n = 4. See also Fig. S1 and Table S1.

Figure 2. Effects of six nDNA-mtDNA *Ant1* and *COI*^{N421A} and *ND6*^{P25L} combination strains on longevity, activity, and thermal tolerance. (**A**) Kaplan Meier analysis of six nDNA-mtDNA combinations. Median lifespan and n are depicted in the chart below. (**B**) Progeroid morphology evident in ANT1 and ANT1 ND6 mice as early kyphosis at 6 mo., which progresses to grey hair, alopecia, and advanced kyphosis at 15 mo. compared to WT and ANT1 COI. (**C**) Indirect calorimetry recordings of activity counts during the dark cycle of all strains at 6 mo. (**D**) Core body temperature for 6 mo. mice measured at 22°C (filled symbols; red box) showing reduction of all *Ant1*-null strains. Core body temperature after 4°C cold stress (hollow symbols; blue box) showing that the ANT1 and ANT1 ND6 strains were unable to maintain normal body temperature

while the ANT1 COI mice were unaffected by cold stress. *p < 0.02 vs. WT; n = 6. See also Fig. S2.

Figure 3. **Progression of cardiomyopathy and left ventricular mechanics in the nDNA-mtDNA combination strains.** **(A)** Correlation between the relative rate of cardiac enlargement (heart weight / body weight) over the lifespan for each strain (p < 0.0001; n = 65 - 111). (**B**) Gross morphology of hearts by H & E stain at 12 mo. of age. (**C**) Cardiac contractility measured by 2-dimensional speckle tracking echocardiography (2D-STE). Speckle-tracking long-axis cardiac strain curves were obtained using Vevostrain software incorporated into Vevo2100 from movies acquired from the B-mode long-axis view of the left ventricle. Representative strain curves obtained from the B-mode long-axis view of the left ventricle over the cardiac cycle (x-axis) showing longitudinal strain (% deformation; y-axis) and region of the left ventricle (z-axis). Each panel shows 49 regional strain curves topographically extending from infero-lateral base (Base $_{Lat.}$) towards LV apex and back towards antero-septal base (Base $_{Sep.}$). Note the progressive variations in magnitude and timing of strain curves between different nDNA-mtDNA combinations. n = 10 – 34. See also Table S2.

Figure 4. **Opposing effects of mtDNA variation in complexes I and IV on mitochondrial morphology and cristae architecture.** Representative electron micrographs of ventricular cardiomyocytes **(A-F)** and mitochondria (**A'-F'**) from each nDNA-mtDNA combination (n = 3); scale bars **A-F**, 2 μm; **A'-F'**, 500 nm. Sarcomeric and mitochondrial alignment in WT (**A**) and COI (**B**) versus structural disarray in all other nDNA-mtDNA combinations (**C-F**). (**B, B'**) Mitochondrial enlargement in COI myocardium. Mitochondrial fragmentation, autophagic vesicles, and lipofuscin accumulation (blue and purple arrows) in ND6 (**C, C'**) and ANT1 ND6 (**F, F'**) myocardium. Mitochondrial proliferation (**D-F**) and cristae abnormalities (**D'-F'**), including cristolysis **D',** ANT1), and reticular morphology (yellow arrow; **E',** ANT1 COI), present in

all *Ant1*-null strains**.** (**G**) Quantification of age-related lipofuscin deposits, normalized to WT. Ultrastructural quantification of mitochondrial content (**H**) and average size (**I**) per strain (n = 496-1541). (**J**) Percentage distribution of mitochondrial size showing the shift in mitochondrial morphology by the ANT1 ND6 compared to WT. (**K**) Percent of abnormal mitochondria counted in each strain. (**L-O**) Average number of mitochondria per mm^2 with the following most common defects in cristae: (**L**) cristolysis, (**M**) reticular, (**N**) partitioning, and (**O**) circular morphologies. *p < 0.05 *vs.* WT; **p < 0.001 *vs.* ANT1 and WT. Data are represented as mean ± S.E. See also Fig. S3 and S4.

Figure 5. Structural and functional consequences of mitochondrial-nuclear interaction on mitochondrial OXPHOS complexes. (**A**) NADH:quinone oxidoreductase (NQR) activity determined by rotenone-sensitive NADH oxidation in the presence of coenzyme Q_1 using isolated heart mitochondria (25 μg) (*p < 0.05 *vs.* age-matched WT; n = 3 - 7). (**B**) Age-dependent decline in complex I diaphorase activity (dOD/min) determined by complex I immunocaptured from 10 μg isolated heart mitochondria (*p < 0.02 *vs.* WT at 6 mo.; **p < 0.0001 *vs.* WT at 6 mo.; & p < 0.05 *vs.* WT at 18 mo.). (**C**) Complex I assembly measured by blue native electrophoresis (BNE) of heart mitochondria (20 μg) and immunodetection with anti-NDUFA1 (n = 2). (**D**) Citrate synthase (CS) activity per mg myocardial tissue as a marker of mitochondrial content at 6 mo. (*p = 0.04; **p < 0.001). (**E**) Cytochrome *c* oxidase (COX) activity from the same samples normalize to CS activity (*p < 0.001). Data are represented as mean ± S.E. (**F**) Resolution of oligomeric states of F_1F_0-ATPase by clear native-PAGE (CN-PAGE). Oligomers were undetectable in *Ant1*$^{-/-}$ mitochondria solubilized in digitonin (3% w/v). V_0 = oligomers, V_d = dimers, V = monomer V*a and V*b = partial complex V components. Each well was loaded with 30 μg of mitochondrial protein, evident by the anti-VDAC loading control from a duplicate gel. n = 3 – 7. See also Fig. S5.

Figure 6. Mitochondrial bioenergetics, ROS production, and mtPTP stability in

isolated cardiac mitochondria from six nDNA-mtDNA genetic combinations. (**A**) Mitochondrial membrane potential determined by TMRM fluorescence respiring on glutamate and malate (GM), graphed relative to WT. (**B**) Mitochondrial oxygen consumption rate metabolizing glutamate and malate (GM) in the absence of ADP or uncoupler (state II or "LEAK" rate). (**C**) Mitochondrial oxygen consumption rate metabolizing GM in the presence of ADP (state III or "P" respiration rate). (**D**) Relative inhibition of respiration by oligomycin in mitochondria respiring on GM in the presence of ADP. (**E**) Hydrogen peroxide (H_2O_2) production detected by Amplex-red in isolated mitochondria incubated with GM, rotenone (R), succinate (Succ) and oligomycin (Oligo) (**F**) Ca^{++} levels required to activate the mtPTP and collapse the mitochondrial membrane potential. Data are represented as mean ± S.E. (**G**) Representative traces of extramitochondrial Ca^{++} following 20 µM Ca^{++} pulses delivered every 2 min to isolated mitochondria until the spontaneous release of mitochondrial Ca^{++}, marking the onset of mtPTP opening in WT and ANT1 ND6 mice. *p ≤ 0.01 *vs*. WT; **p ≤ 0.01 *vs*. ANT1; n = 3 - 5. See also Fig. S6.

Figure 7. Effect of mitochondrial-nuclear interaction on somatic mtDNA mutation accumulation and caspase activation. (**A-B**) Long-range amplification of mtDNA (12.7kb) from each nDNA-mtDNA combination at 12 -15 mo. indicating multiple, large-scale deletions. (**C**) Activation of intrinsic apoptosis determined by effector caspase 3 & 7 activities, Data are represented as mean ± S.E. *p < 0.001; n = 4. See also Fig. S7.

References

Arbustini, E., Diegoli, M., Fasani, R., Grasso, M., Morbini, P., Banchieri, N., Bellini, O., Dal Bello, B., Pilotto, A., Magrini, G., et al. (1998a). Mitochondrial DNA mutations and mitochondrial abnormalities in dilated cardiomyopathy. Am. J. Pathol. *153*, 1501-1510.

Arbustini, E., Fasani, R., Morbini, P., Diegoli, M., Grasso, M., Dal Bello, B., Marangoni, E., Banfi, P., Banchieri, N., Bellini, O., et al. (1998b). Coexistence of mitochondrial DNA and beta myosin heavy chain mutations in hypertrophic cardiomyopathy with late congestive heart failure [published erratum appears in Heart 1999 Mar;81(3):330]. Heart *80*, 548-558.

Aronow, B.J., Toyokawa, T., Canning, A., Haghighi, K., Delling, U., Kranias, E., Molkentin, J.D., and Dorn, G.W., 2nd (2001). Divergent transcriptional responses to independent genetic causes of cardiac hypertrophy. Physiol. Genomics *6*, 19-28.

Bauer, M.K., Schubert, A., Rocks, O., and Grimm, S. (1999). Adenine nucleotide translocase-1, a component of the permeability transition pore, can dominantly induce apoptosis. J. Cell Biol. *147*, 1493-1502.

Biering-Sorensen, T., Biering-Sorensen, S.R., Olsen, F.J., Sengelov, M., Jorgensen, P.G., Mogelvang, R., Shah, A.M., and Jensen, J.S. (2017). Global longitudinal strain by echocardiography predicts long-term risk of cardiovascular morbidity and mortality in a low-risk general population: The Copenhagen City Heart Study. Circ. Cardiovasc. Imaging *10*, e005521.

Brand, M.D. (2010). The sites and topology of mitochondrial superoxide production. Exp. Gerontol. *45*, 466-472.

Brand, M.D., Pakay, J.L., Ocloo, A., Kokoszka, J., Wallace, D.C., Brookes, P.S., and Cornwall, E.J. (2005). The basal proton conductance of mitochondria depends on adenine nucleotide translocase content. Biochem. J. *392*, 353-362.

Burke, M.A., Chang, S., Wakimoto, H., Gorham, J.M., Conner, D.A., Christodoulou, D.C., Parfenov, M.G., DePalma, S.R., Eminaga, S., Konno, T., et al. (2016). Molecular profiling of dilated cardiomyopathy that progresses to heart failure. JCI Insight *1*, e86898.

Cadete, V.J.J., Deschênes, S., Cuillerier, A., Brisebois, F., Sugiura, A., Vincent, A., Turnbull, D., Picard, M., McBride, H.M., and Burelle, Y. (2016). Formation of mitochondrial-derived vesicles is an active and physiologically relevant mitochondrial quality control process in the cardiac system. J. Physiol. *594*, 5343-5362.

Cannon, B., and Nedergaard, J. (2011). Nonshivering thermogenesis and its adequate measurement in metabolic studies. J. Exp. Biol. *214*, 242-253.

Capaldi, R.A., Marusich, M.F., and Taanman, J.W. (1995). Mammalian cytochrome-c oxidase: characterization of enzyme and immunological detection of subunits in tissue extracts and whole cells. Methods Enzymol. *260*, 117-132.

Carrozzo, R., Wittig, I., Santorelli, F.M., Bertini, E., Hofmann, S., Brandt, U., and Schagger, H. (2006). Subcomplexes of human ATP synthase mark mitochondrial biosynthesis disorders. Ann. Neurol. *59*, 265-275.

Chen, H., Vermulst, M., Wang, Y.E., Chomyn, A., Prolla, T.A., McCaffery, J.M., and Chan, D.C. (2010). Mitochondrial fusion is required for mtDNA stability in skeletal muscle and tolerance of mtDNA mutations. Cell *141*, 280-289.

Chevrollier, A., Loiseau, D., Reynier, P., and Stepien, G. (2011). Adenine nucleotide translocase 2 is a key mitochondrial protein in cancer metabolism. Biochim. Biophys. Acta. *1807*, 562-567.

Chouchani, E.T., Pell, V.R., Gaude, E., Aksentijevic, D., Sundier, S.Y., Robb, E.L., Logan, A., Nadtochiy, S.M., Ord, E.N., Smith, A.C., et al. (2014). Ischaemic

accumulation of succinate controls reperfusion injury through mitochondrial ROS. Nature *515*, 431-435.

Cogliati, S., Enriquez, J.A., and Scorrano, L. (2016). Mitochondrial cristae: where beauty meets functionality. Trends Biochem. Sci. *41*, 261-273.

Dai, D.F., Chen, T., Wanagat, J., Laflamme, M., Marcinek, D.J., Emond, M.J., Ngo, C.P., Prolla, T.A., and Rabinovitch, P.S. (2010). Age-dependent cardiomyopathy in mitochondrial mutator mice is attenuated by overexpression of catalase targeted to mitochondria. Aging Cell *9*, 536-544.

Davies, K.M., Anselmi, C., Wittig, I., Faraldo-Gomez, J.D., and Kuhlbrandt, W. (2012). Structure of the yeast F1Fo-ATP synthase dimer and its role in shaping the mitochondrial cristae. Proc. Natl. Acad. Sci. USA *109*, 13602-13607.

Ding, W.X., Guo, F., Ni, H.M., Bockus, A., Manley, S., Stolz, D.B., Eskelinen, E.L., Jaeschke, H., and Yin, X.M. (2012). Parkin and mitofusins reciprocally regulate mitophagy and mitochondrial spheroid formation. The Journal of biological chemistry *287*, 42379-42388.

Duckles, S.P., Krause, D.N., Stirone, C., and Procaccio, V. (2006). Estrogen and mitochondria: a new paradigm for vascular protection? Mol. Interv. *6*, 26-35.

Echaniz-Laguna, A., Chassagne, M., Ceresuela, J., Rouvet, I., Padet, S., Acquaviva, C., Nataf, S., Vinzio, S., Bozon, D., and Mousson de Camaret, B. (2012). Complete loss of expression of the ANT1 gene causing cardiomyopathy and myopathy. J. Med. Genet. *49*, 146-150.

Eichner, L.J., and Giguere, V. (2011). Estrogen related receptors (ERRs): a new dawn in transcriptional control of mitochondrial gene networks. Mitochondrion *11*, 544-552.

Fan, W., Waymire, K., Narula, N., Li, P., Rocher, C., Coskun, P.E., Vannan, M.A., Narula, J., MacGregor, G.R., and Wallace, D.C. (2008). A mouse model of mitochondrial disease reveals germline selection against severe mtDNA mutations. Science *319*, 958-962.

Freeman, H.C., Hugill, A., Dear, N.T., Ashcroft, F.M., and Cox, R.D. (2006). Deletion of nicotinamide nucleotide transhydrogenase: a new quantitive trait locus accounting for glucose intolerance in C57BL/6J mice. Diabetes *55*, 2153-2156.

Geyer, H., Caracciolo, G., Abe, H., Wilansky, S., Carerj, S., Gentile, F., Nesser, H.J., Khandheria, B., Narula, J., and Sengupta, P.P. (2010). Assessment of myocardial mechanics using speckle tracking echocardiography: fundamentals and clinical applications. J. Am. Soc. Echocardiogr. *23*, 351-369; quiz 453-355.

Graham, B.H., Waymire, K.G., Cottrell, B., Trounce, I.A., MacGregor, G.R., and Wallace, D.C. (1997). A mouse model for mitochondrial myopathy and cardiomyopathy resulting from a deficiency in the heart/skeletal muscle isoform of the adenine nucleotide translocator. Nat. Genet. *16*, 226-234.

Houtkooper, R.H., Argmann, C., Houten, S.M., Canto, C., Jeninga, E.H., Andreux, P.A., Thomas, C., Doenlen, R., Schoonjans, K., and Auwerx, J. (2011). The metabolic footprint of aging in mice. Sci. Rep. *1*, 134.

Huang, T.T., Naeemuddin, M., Elchuri, S., Yamaguchi, M., Kozy, H.M., Carlson, E.J., and Epstein, C.J. (2006). Genetic modifiers of the phenotype of mice deficient in mitochondrial superoxide dismutase. Hum. Mol. Genet. *15*, 1187-1194.

Jang, J.Y., Choi, Y., Jeon, Y.K., Aung, K.C., and Kim, C.W. (2008). Over-expression of adenine nucleotide translocase 1 (ANT1) induces apoptosis and tumor regression in vivo. BMC cancer *8*, 160.

Ji, F., Sharpley, M.S., Derbeneva, O., Alves, L.S., Qian, P., Wang, Y., Chalkia, D., Lvova, M., Xu, J., Yao, W., et al. (2012). Mitochondrial DNA variant associated with Leber hereditary optic neuropathy and high-altitude Tibetans. Proc. Natl. Acad. Sci. USA *109*, 7391-7396.

Ji, Y., Liang, M., Zhang, J., Zhang, M., Zhu, J., Meng, X., Zhang, S., Gao, M., Zhao, F., Wei, Q.P., et al. (2014). Mitochondrial haplotypes may modulate the phenotypic manifestation of the LHON-associated ND1 G3460A mutation in Chinese families. J. Hum. Genet. *59*, 134-140.

Kim, A., Chen, C.H., Ursell, P., and Huang, T.T. (2010). Genetic modifier of mitochondrial superoxide dismutase-deficient mice delays heart failure and prolongs survival. Mamm. Genome *21*, 534-542.

Kokoszka, J.E., Waymire, K.G., Flierl, A., Sweeney, K.M., Angelin, A., MacGregor, G.R., and Wallace, D.C. (2016). Deficiency in the mouse mitochondrial adenine nucleotide translocator isoform 2 gene is associated with cardiac noncompaction. Biochim. Biophys. Acta. *1857*, 1203-1212.

Kokoszka, J.E., Waymire, K.G., Levy, S.E., Sligh, J.E., Cai, J., Jones, D.P., MacGregor, G.R., and Wallace, D.C. (2004). The ADP/ATP translocator is not essential for the mitochondrial permeability transition pore. Nature *427*, 461-465.

Lin, C.S., Sharpley, M.S., Fan, W., Waymire, K.G., Sadun, A., Carelli, V., Ross-Cisneros, F.N., Baciu, P., Sung, E., McManus, M.J., et al. (2012). A mouse mtDNA mutant model of Leber's Hereditary Optic Neuropathy. Proc. Natl. Acad. Sci. USA *109*, 20065-20070.

Mofarrahi, M., Guo, Y., Haspel, J.A., Choi, A.M., Davis, E.C., Gouspillou, G., Hepple, R.T., Godin, R., Burelle, Y., and Hussain, S.N. (2013). Autophagic flux and oxidative capacity of skeletal muscles during acute starvation. Autophagy *9*, 1604-1620.

Mott, J.L., Zhang, D., Freeman, J.C., Mikolajczak, P., Chang, S.W., and Zassenhaus, H.P. (2004). Cardiac disease due to random mitochondrial DNA mutations is prevented by cyclosporin A. Biochem. Biophys. Res. Commun. *319*, 1210-1215.

Mourier, A., Ruzzenente, B., Brandt, T., Kuhlbrandt, W., and Larsson, N.G. (2014). Loss of LRPPRC causes ATP synthase deficiency. Hum. Mol. Genet. *23*, 2580-2592.

Murphy, E., Ardehali, H., Balaban, R.S., DiLisa, F., Dorn, G.W., II, Kitsis, R.N., Otsu, K., Ping, P., Rizzuto, R., Sack, M.N., et al. (2016). AHA position paper on mitochondrial function, biology and role in disease. J. Am. Heart Assoc., *118*; 1960-1991.

Murphy, M.P. (2009). How mitochondria produce reactive oxygen species. Biochem. J. *417*, 1-13.

Narula, N., Zaragoza, M.V., Sengupta, P.P., Li, P., Haider, N., Verjans, J., Waymire, K., Vannan, M., and Wallace, D.C. (2011). Adenine nucleotide translocase 1 deficiency results in dilated cardiomyopathy with defects in myocardial mechanics, histopathological alterations, and activation of apoptosis. JACC Cardiovasc. Imaging *4*, 1-10.

Navarro, S.J., Trinh, T., Lucas, C.A., Ross, A.J., Waymire, K.G., and Macgregor, G.R. (2012). The C57BL/6J mouse strain background modifies the effect of a mutation in Bcl2l2. G3 (Bethesda) *2*, 99-102.

Palmer, J.W., Tandler, B., and Hoppel, C.L. (1977). Biochemical properties of subsarcolemmal and interfibrillar mitochondria isolated from rat cardiac muscle. J. Biol. Chem. *252*, 8731-8739.

Palmieri, L., Alberio, S., Pisano, I., Lodi, T., Meznaric-Petrusa, M., Zidar, J., Santoro, A., Scarcia, P., Fontanesi, F., Lamantea, E., et al. (2005). Complete loss-of-function of the heart/muscle-specific adenine nucleotide translocator is associated with mitochondrial myopathy and cardiomyopathy. Hum. Mol. Genet. *14*, 3079-3088.

Paumard, P., Vaillier, J., Coulary, B., Schaeffer, J., Soubannier, V., Mueller, D.M., Brethes, D., di Rago, J.P., and Velours, J. (2002). The ATP synthase is involved in generating mitochondrial cristae morphology. EMBO J. *21*, 221-230.

Picard, M., McManus, M.J., Csordas, G., Varnai, P., Dorn Ii, G.W., Williams, D., Hajnoczky, G., and Wallace, D.C. (2015). Trans-mitochondrial coordination of cristae at regulated membrane junctions. Nat. Commun. *6*, 6259.

Porter, G.A., Jr., Hom, J., Hoffman, D., Quintanilla, R., de Mesy Bentley, K., and Sheu, S.S. (2011). Bioenergetics, mitochondria, and cardiac myocyte differentiation. Prog. Pediatr. Cardiol. *31*, 75-81.

Scialo, F., Sriram, A., Fernandez-Ayala, D., Gubina, N., Lohmus, M., Nelson, G., Logan, A., Cooper, H.M., Navas, P., Enriquez, J.A., et al. (2016). Mitochondrial ROS produced via reverse electron transport extend animal lifespan. Cell Metab. *23*, 725-734.

Strauss, K.A., Dubiner, L., Simon, M., Zaragoza, M., Sengupta, P.P., Li, P., Narula, N., Dreike, S., Platt, J., Procaccio, V., et al. (2013). Severity of cardiomyopathy associated with adenine nucleotide translocator-1 deficiency correlates with mtDNA haplogroup. Proc. Natl. Acad. Sci. USA *110*, 3253-3458.

Strauss, M., Hofhaus, G., Schroder, R.R., and Kuhlbrandt, W. (2008). Dimer ribbons of ATP synthase shape the inner mitochondrial membrane. EMBO J. *27*, 1154-1160.

Tiepolo, T., Angelin, A., Palma, E., Sabatelli, P., Merlini, L., Nicolosi, L., Finetti, F., Braghetta, P., Vuagniaux, G., Dumont, J.M., et al. (2009). The cyclophilin inhibitor Debio 025 normalizes mitochondrial function, muscle apoptosis and ultrastructural defects in Col6a1-/- myopathic mice. Br. J. Pharmacol. *157*, 1045-1052.

Toye, A.A., Lippiat, J.D., Proks, P., Shimomura, K., Bentley, L., Hugill, A., Mijat, V., Goldsworthy, M., Moir, L., Haynes, A., et al. (2005). A genetic and physiological study of impaired glucose homeostasis control in C57BL/6J mice. Diabetologia *48*, 675-686.

van der Westhuizen, F.H., Smet, J., Levanets, O., Meissner-Roloff, M., Louw, R., Van Coster, R., and Smuts, I. (2010). Aberrant synthesis of ATP synthase resulting from a novel deletion in mitochondrial DNA in an African patient with progressive external ophthalmoplegia. J. Inherit. Metab. Dis. *33 Suppl 3*, S55-562.

Vermulst, M., Bielas, J.H., Kujoth, G.C., Ladiges, W.C., Rabinovitch, P.S., Prolla, T.A., and Loeb, L.A. (2007). Mitochondrial point mutations do not limit the natural lifespan of mice. Nat. Genet. *39*, 540-543.

Vermulst, M., Bielas, J.H., and Loeb, L.A. (2008a). Quantification of random mutations in the mitochondrial genome. Methods *46*, 263-268.

Vermulst, M., Wanagat, J., Kujoth, G.C., Bielas, J.H., Rabinovitch, P.S., Prolla, T.A., and Loeb, L.A. (2008b). DNA deletions and clonal mutations drive premature aging in mitochondrial mutator mice. Nat. Genet. *40*, 392-394.

Wallace, D.C. (2013a). Bioenergetics in human evolution and disease:Implications for the origins of biological complexity and the missing genetic variation of common diseases. Philos. Trans. R. Soc. Lond. B Biol. Sci. *368*, 20120267.

Wallace, D.C. (2013b). Mitochondrial bioenergetic etiology of disease. J. Clin. Invest. *123*, 1405-1412.

Wallace, D.C., Lott, M.T., and Procaccio, V. (2013). Mitochondrial Medicine: The Mitochondrial Biology and Genetics of Metabolic and Degenerative Diseases, Cancer, and Aging. In Emery and Rimoin's Principles and Practice of Medical Genetics. D.L. Rimoin, R.E. Pyeritz, and B.R. Korf, eds. (Philadelphia: Churchill Livingstone Elsevier).

Wittig, I., Karas, M., and Schagger, H. (2007). High resolution clear native electrophoresis for in-gel functional assays and fluorescence studies of membrane protein complexes. Mol. Cell. Proteomics *6*, 1215-1225.

Wittig, I., Meyer, B., Heide, H., Steger, M., Bleier, L., Wumaier, Z., Karas, M., and Schagger, H. (2010). Assembly and oligomerization of human ATP synthase lacking mitochondrial subunits a and A6L. Biochim. Biophys. Acta. *1797*, 1004-1011.

Yadava, N., Potluri, P., Smith, E.N., Bisevac, A., and Scheffler, I.E. (2002). Species-specific and mutant MWFE proteins. Their effect on the assembly of a functional mammalian mitochondrial complex I. J. Biol. Chem. *277*, 21221-21230.

Yu, T., Sheu, S.S., Robotham, J.L., and Yoon, Y. (2008). Mitochondrial fission mediates high glucose-induced cell death through elevated production of reactive oxygen species. Cardiovasc. Res. *79*, 341-351.

Zamora, M., Granell, M., Mampel, T., and Vinas, O. (2004a). Adenine nucleotide translocase 3 (ANT3) overexpression induces apoptosis in cultured cells. FEBS Lett. *563*, 155-160.

Zamora, M., Merono, C., Vinas, O., and Mampel, T. (2004b). Recruitment of NF-kappaB into mitochondria is involved in adenine nucleotide translocase 1 (ANT1)-induced apoptosis. J. Biol. Chem. *279*, 38415-38423.

Zaragoza, M.V., Brandon, M.C., Diegoli, M., Arbustini, E., and Wallace, D.C. (2011). Mitochondrial cardiomyopathies: how to identify candidate pathogenic mutations by mitochondrial DNA sequencing, MITOMASTER and phylogeny. Eur. J. Hum. Genet. *19*, 200-207.

Zorov, D.B., Filburn, C.R., Klotz, L.O., Zweier, J.L., and Sollott, S.J. (2000). Reactive oxygen species (ROS)-induced ROS release: a new phenomenon accompanying induction of the mitochondrial permeability transition in cardiac myocytes. J. Exp. Med. *192*, 1001-1014.
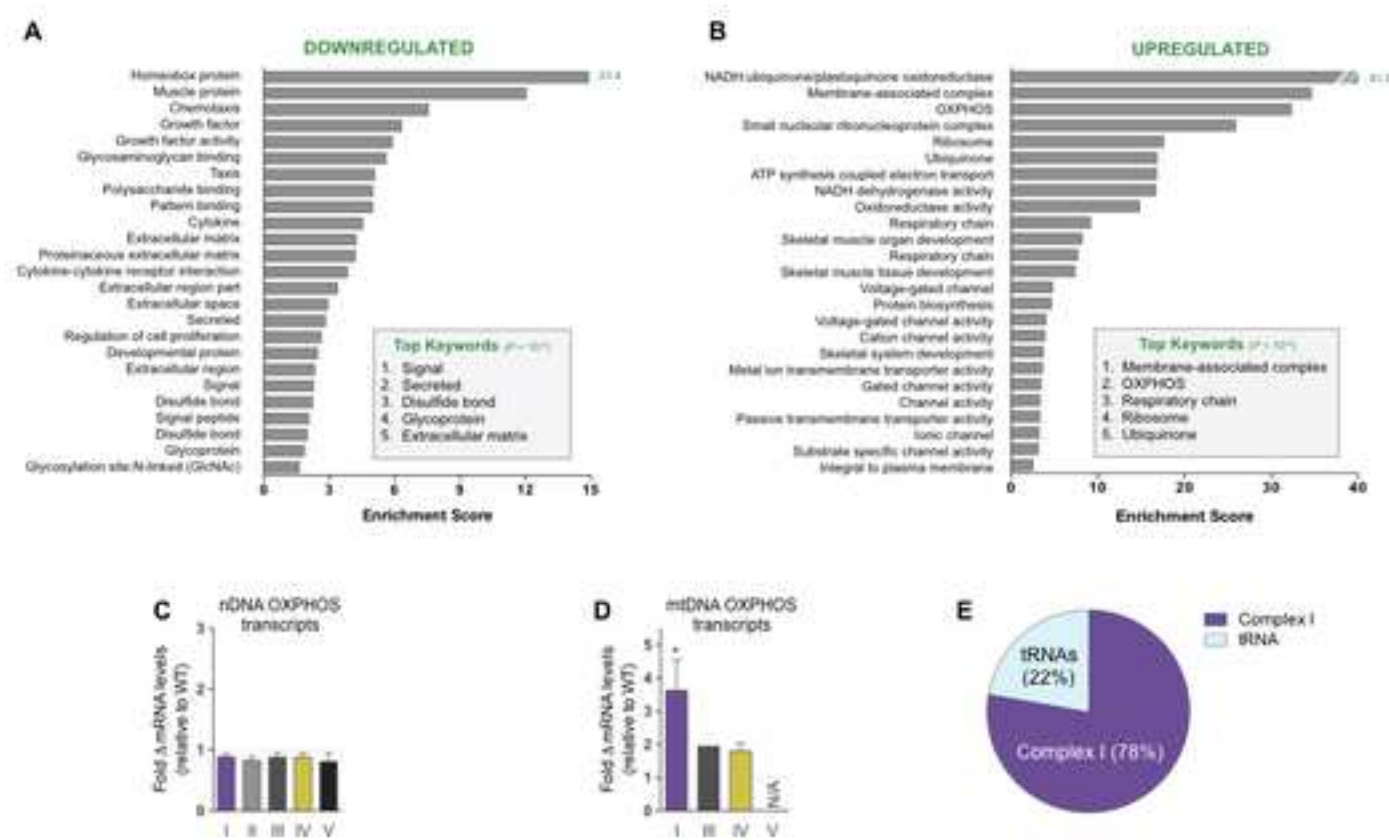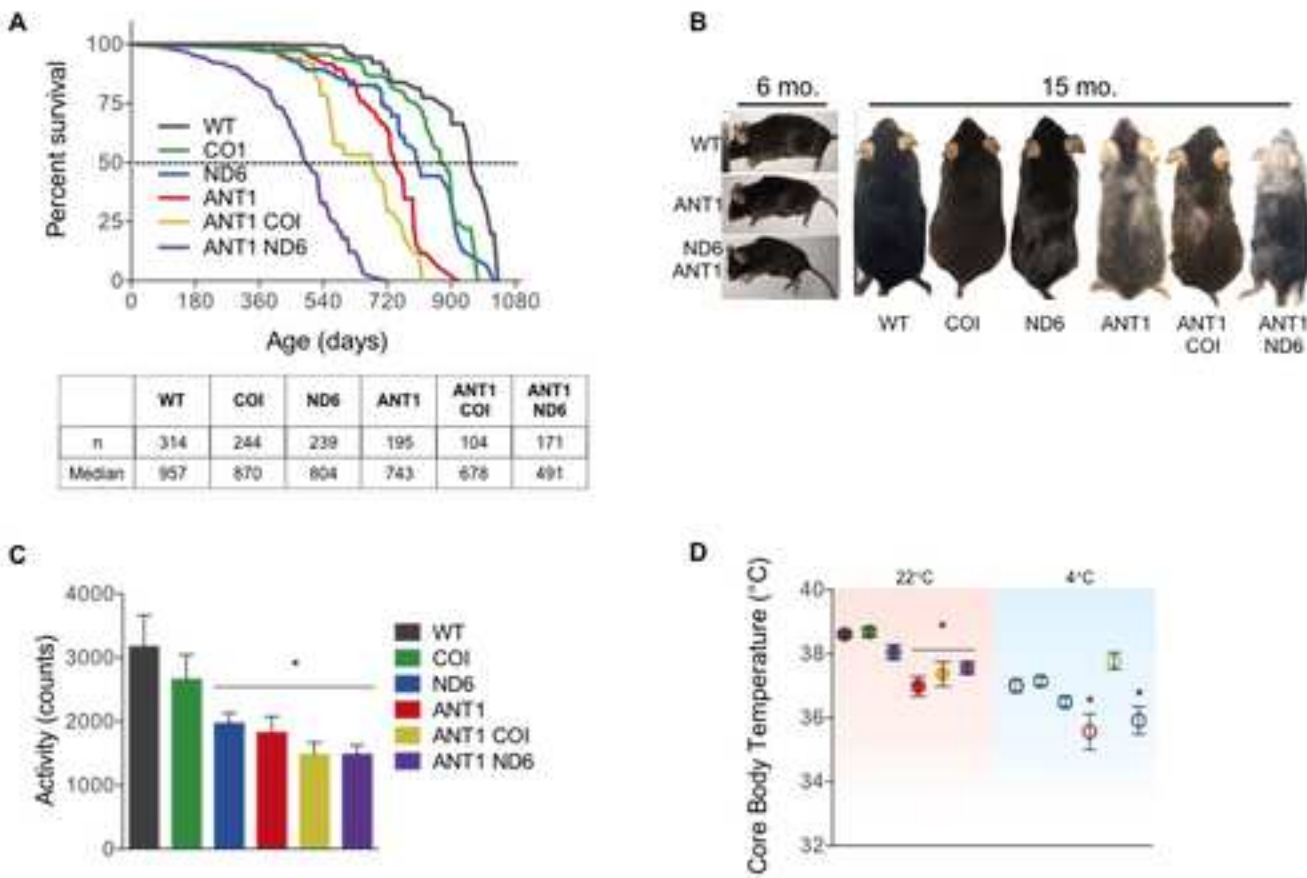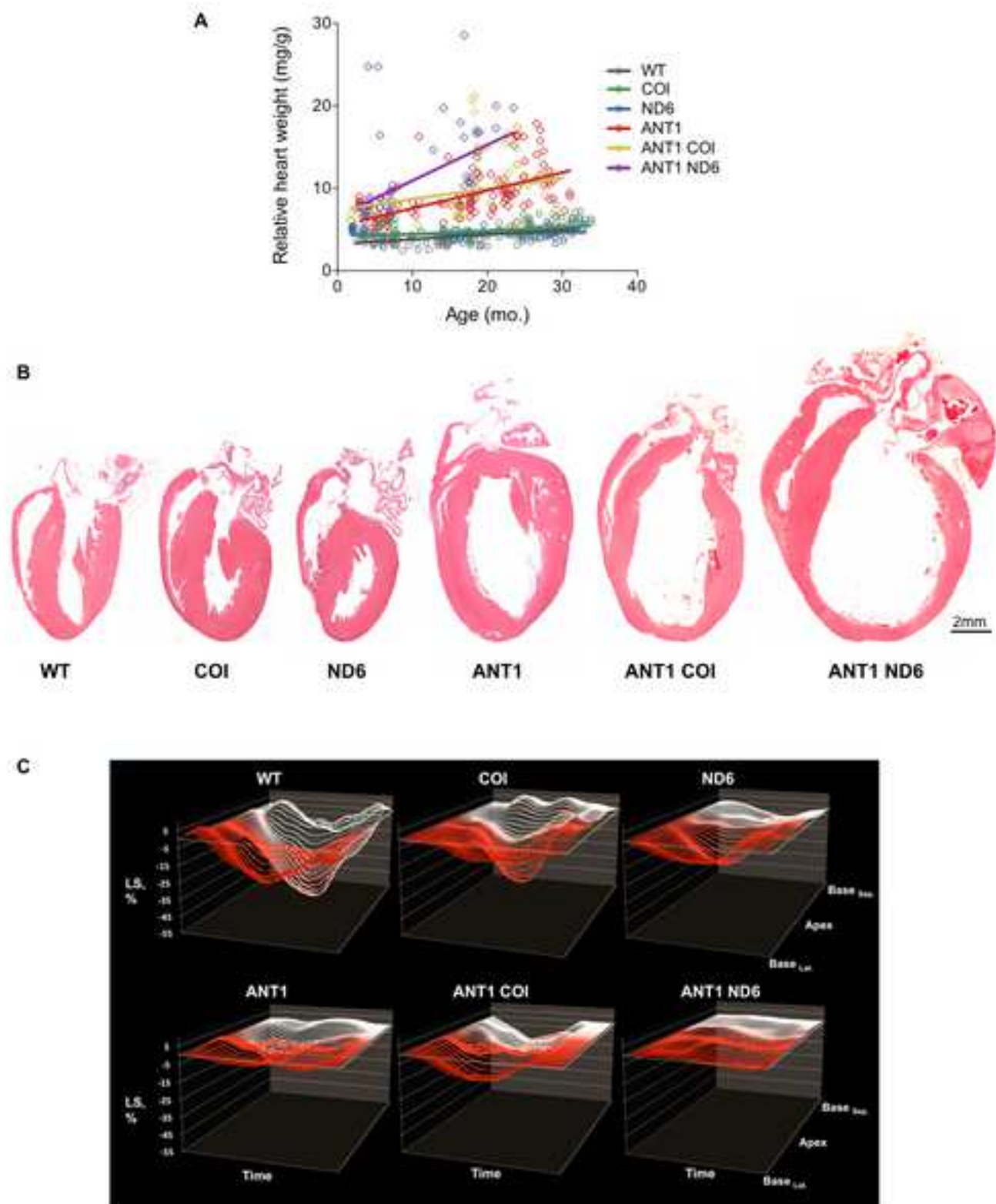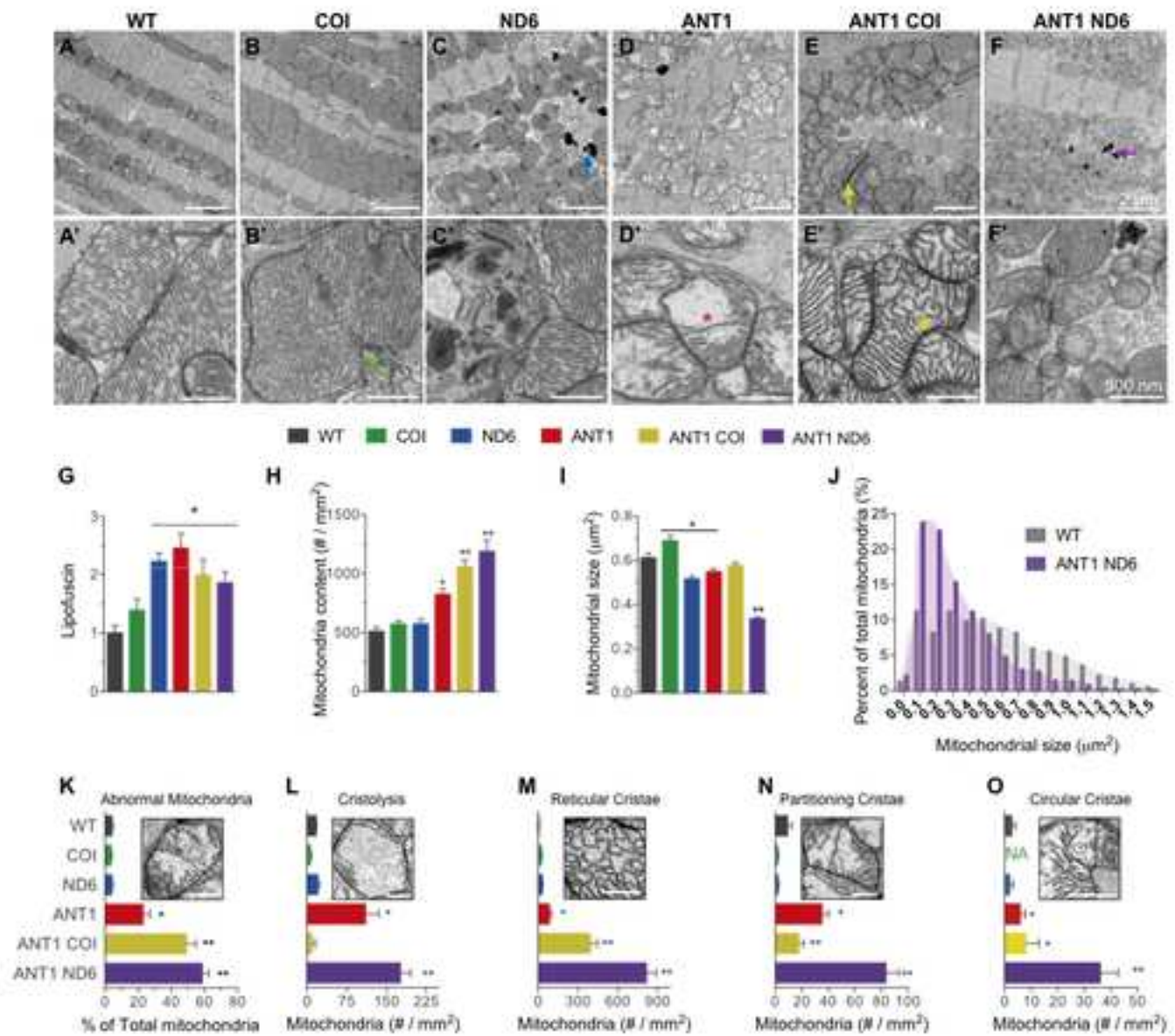
FIGURE 1

Figure 2

FIGURE 2

Figure 3

A

B

C

FIGURE 3

Figure 4

FIGURE 4
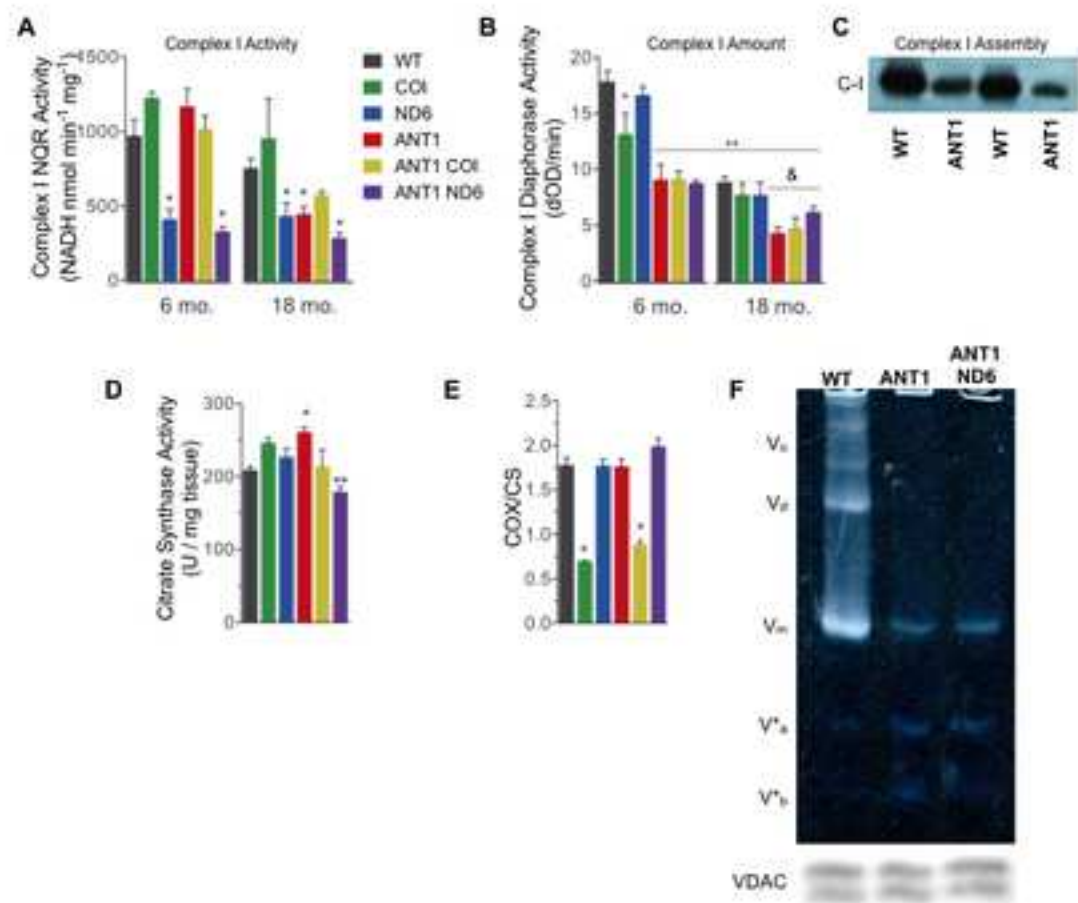
Figure 5

FIGURE 5

Figure 6
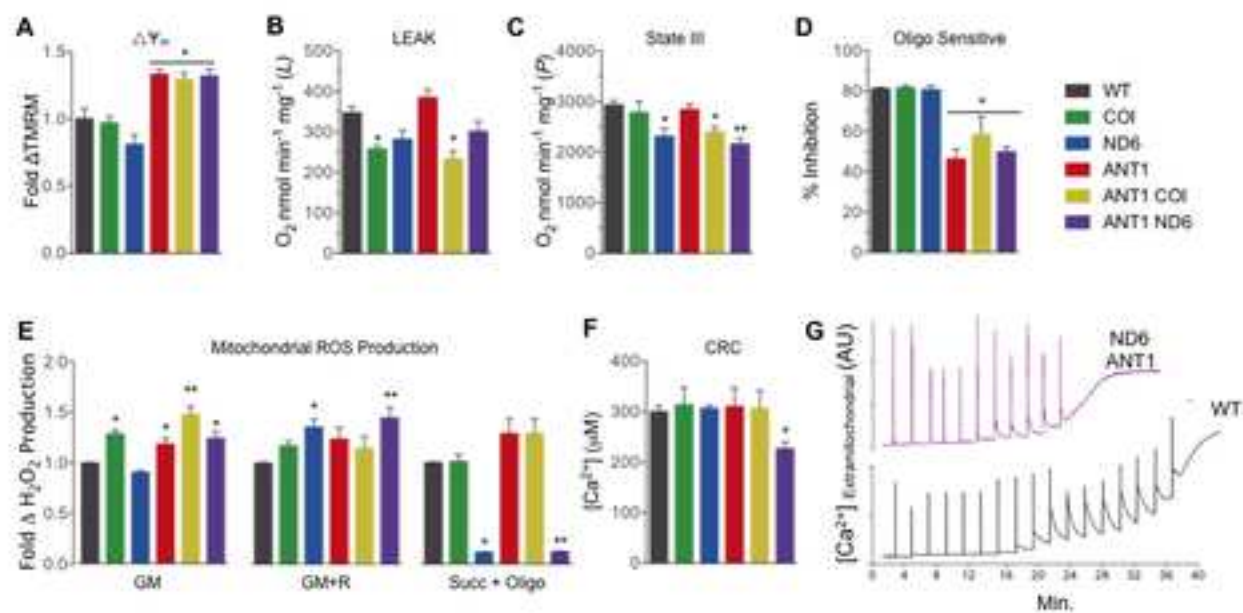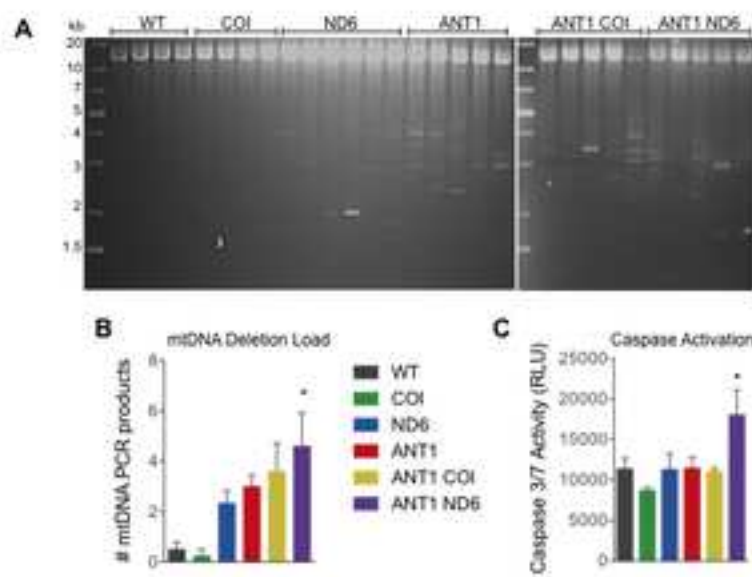
FIGURE 6

Figure 7

FIGURE 7

Supplemental Information

Figure and Table Legends

Figure S1. Related to Figure 1: Integrative analysis by clustering of functional annotation terms. Functional cluster analysis revealed significant repression of pathways associated with extracellular matrix maintenance and signaling, structural protein binding, and cell chemotaxis and migration signaling, which together contribute to organ pattern formation. The overexpression of contractile and fibrous components specific to skeletal muscle, cartilage and bone development also mark the loss of myocardial integrity and increased fibrosis observed in cardiac remodeling of the *Ant1*-null heart.

Figure S2. Related to Figure 2: Average body weight per strain. Body weights are indistinguishable between strains of age-matched mice that underwent indirect calorimetry screening at 6 mo. (p ≥ 0.56).

Figure S3. Related to Figure 4: Effect of mitochondrial mutations on mitochondrial size distribution. Histograms reveal the diametrically opposed influence of mtDNA *ND6*[P25L] and *COI*[V421A] variants on mitochondrial size. *ND6*[P25L] causes mitochondrial fragmentation, and acts synergistically with nDNA *Ant*^{-/-}, reducing most mitochondria to 0.2 um^2. *COI*[V421A] increases mitochondrial size up to 3.0 um^2, and brings *Ant*^{-/-} mitochondria back within WT range (0 - 2.4 um^2).

Figure S4. Related to Figure 4: Intramitochondrial abnormalities caused by loss of ANT1. (**A-B**) Fission-associated partitioning cristae (yellow tracings) divide defective, hypodense regions (yellow shading, **B**) with circular cristae (red shading, **A**). Yellow arrows (**B**) highlight fission-associated pinching of the OMM. **C-E.** Intramitochondrial inclusions formed by paracrystalline cristae (**C**) or aggregates of malformed cristae (**D**), or compartmentalized by an inner membrane boundary (**E**). (**F**) Dense packing of circular cristae into concentric inclusions (orange arrows). Mitochondrial release of concentric membrane components (purple arrow) into the cytoplasm, possibly for degradation (**G**) or signaling as mitochondrial-derived vesicles (**H**; red arrow, (Cadete et al., 2016). Membrane-bound hypodense regions (blue arrows), which may represent mitochondrial spheroids (**I**; (Ding et al., 2012) or cristolysis (**J**). Scale bars (red) = 500nm.

Figure S5. Related to Figure 5: F₁Fₒ-ATPase structural assembly. Clear native electrophoresis (CNE) of maltoside-solubilized (2.5% w/v) heart mitochondria (50 µg) showing loss of ANT1 destabilizes the F_1F_o-ATPase holo-complex (V_m) by the appearance of lower molecular weight subcomplexes (V*a, V*b) (n = 3).

Figure S6. Related to Figure 6: mtDNA *COI*[V421A] prevents the decline in mitochondrial function due to loss of *Ant1*^{-/-} in the aged heart. The respiratory control ratio (RCR) is shown as the ratio of ADP-stimulated to *LEAK* (*P:L*) states from cardiac mitochondria isolated from mice at 18mo. of age (*****p < 0.05 vs. WT; n = 3 – 5).

Figure S7. Related to Figure 7: mtDNA deletions increase with age and correlate with disease progression. (A) Average frequency of deletions detected by qPCR of the most common deletion hotspot flanking two 15-bp repeats in mtDNA, depicted as fold change from WT at 6 - 9 mo. of age (*p < 0.01; n = 4 - 6). Correlation between the median lifespan (**B**) or cardiac function (**C**) of each strain and total mtDNA deletion load determined by LX-PCR at 12 - 15 mo.

Table S1. **Related to Figure 1.** Total mtRNA and nRNA-OXPHOS transcripts detected by RNASeq analysis from the left ventricle, shown as fold change (bold) of ANT1 from WT age-matched control, and the adjusted p value.

Table 2. Related to Figure 3. Echocardiographic parameters. Data are expressed as mean ± standard deviation (S. D.); *p ≤ 0.03 *vs*. WT; ♦p ≤ 0.03 *vs*. ANT1. Abbreviations: SepTd, septal thickness at diastole; LVDD, left ventricular diastolic diameter; PWTd, Posterior wall thickness diastole; SepTs, septal thickness at systole; LVSD left ventricular systolic diameter; FS, fractional shortening; EF, ejection fraction; LV, left ventricle; RWT, relative wall thickness.
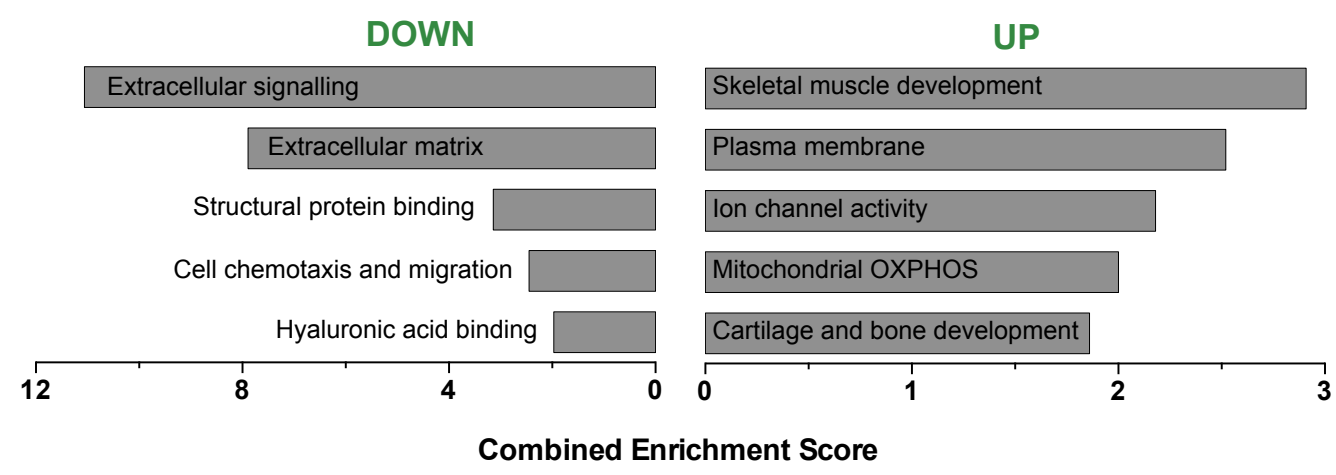
Figure S1
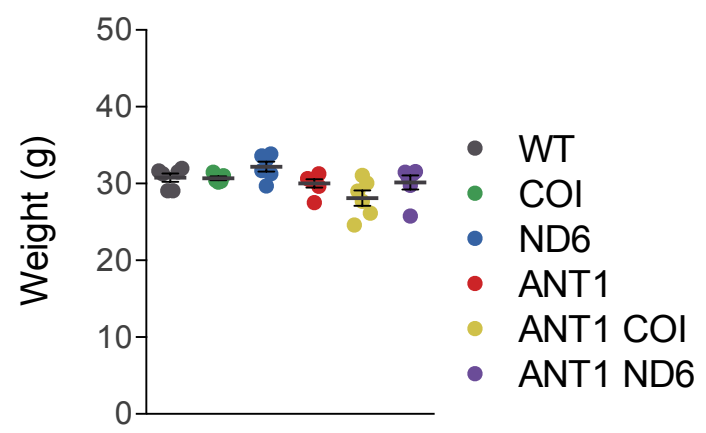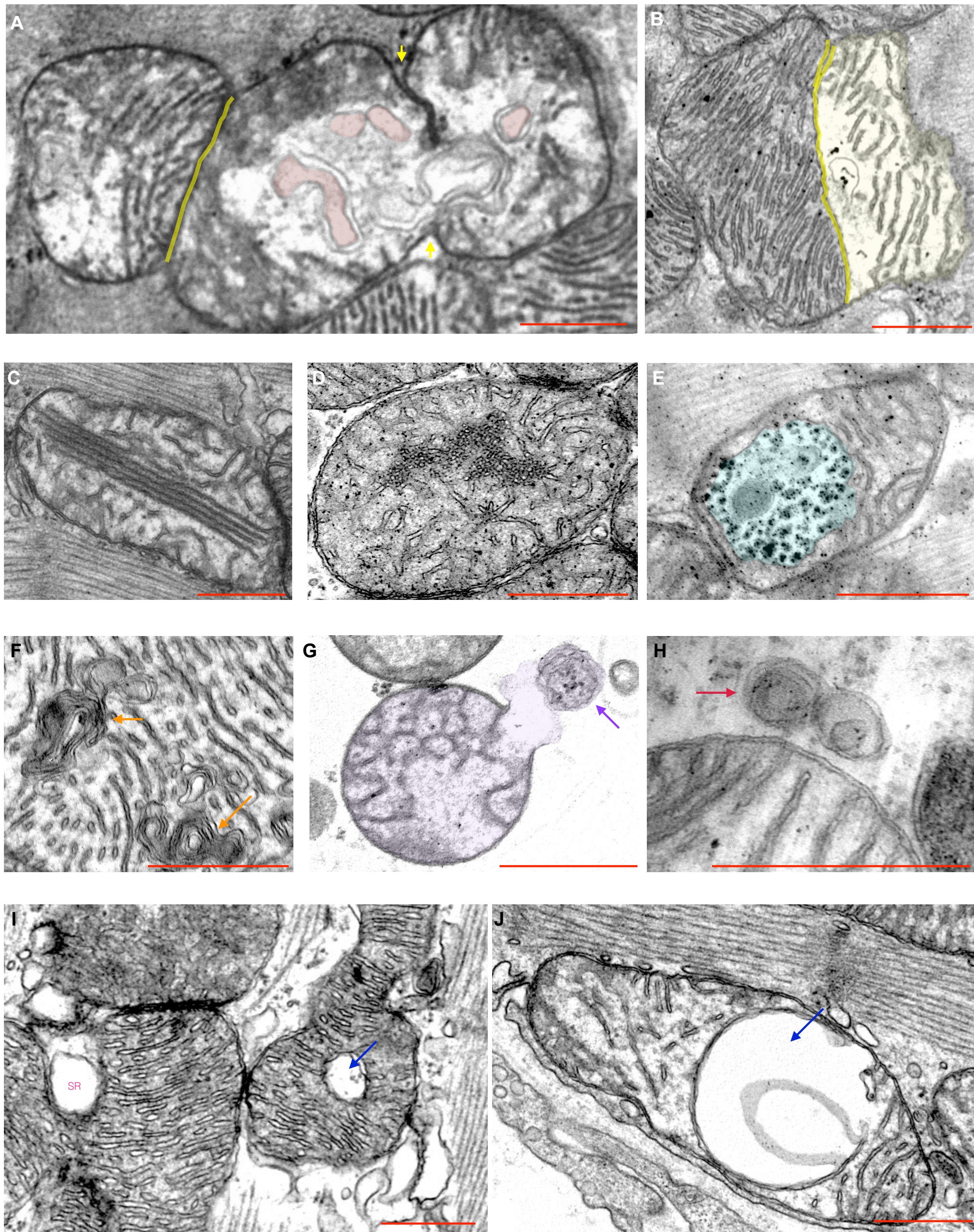
Figure S2
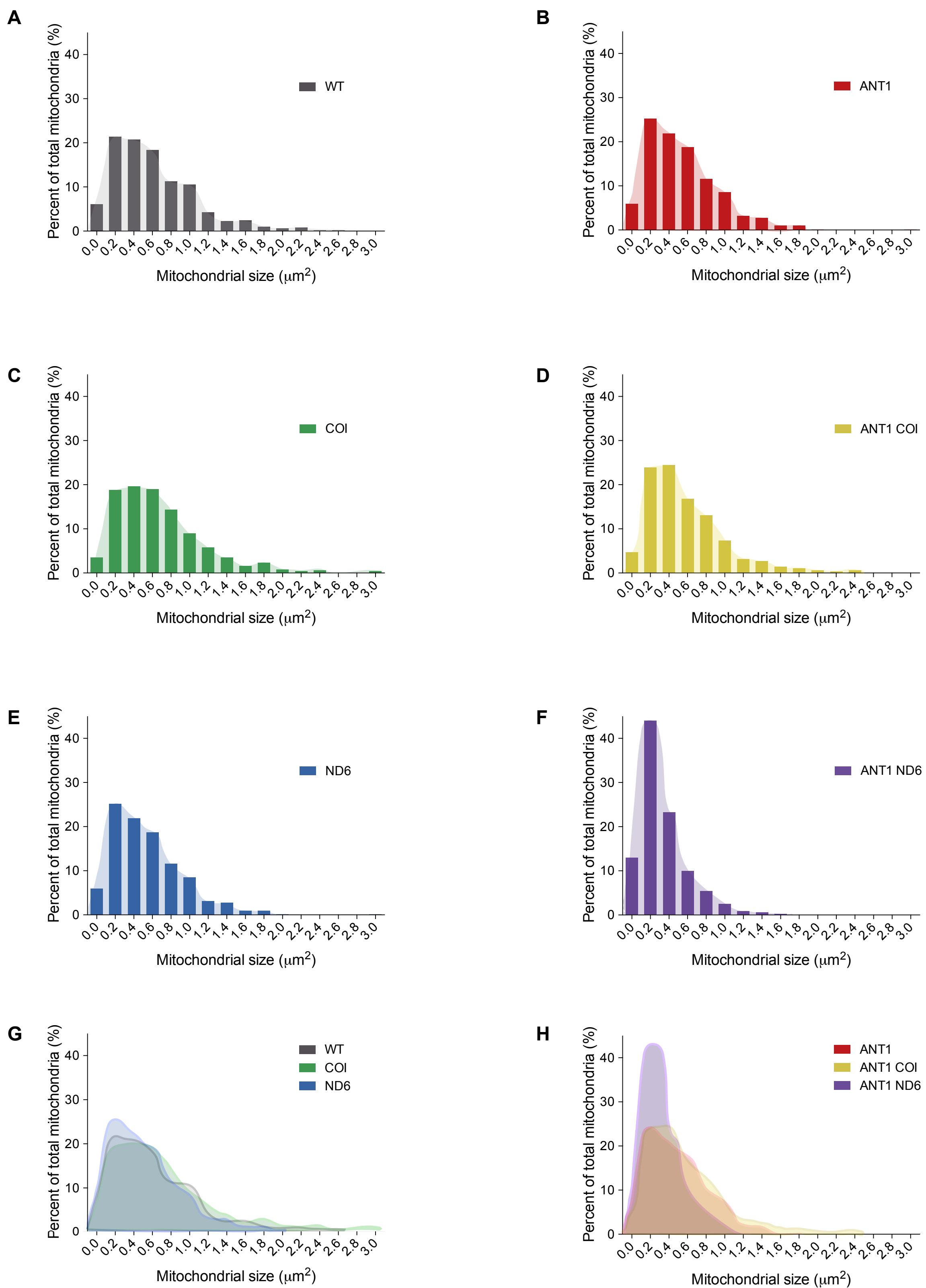
Figure S3

Figure S4

Figure S5

Figure S6

A

Fold Δ mtDNA deletions

- WT
- COI
- ND6
- ANT1
- ANT1 COI
- ANT1 ND6

*

B

Median lifespan (mo.)

R² = 0.879
p = 0.006

mtDNA deletions

C

Ejection Fraction (%)

R² = 0.804
p = 0.015

mtDNA deletions
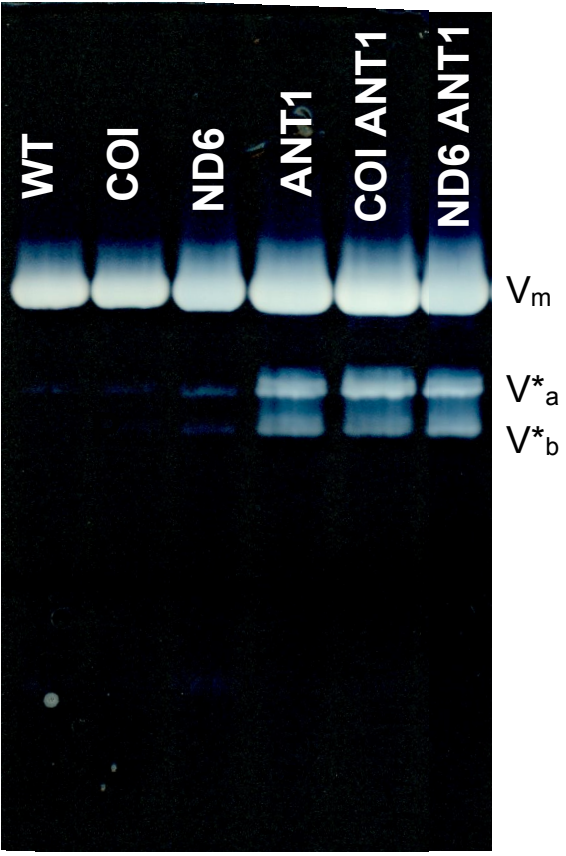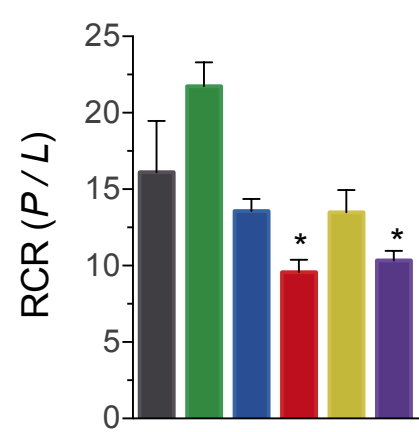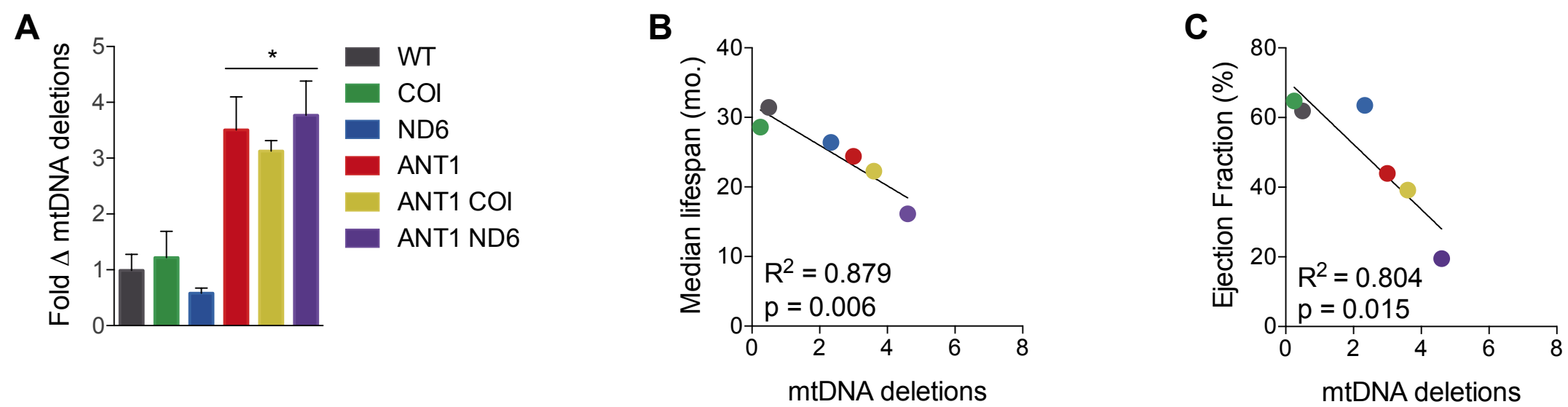
Figure S7

Table S1. Related to Figure 1.

nDNA Gene	Fold Δ	p adj	mtDNA Gene	Fold Δ	p adj
Ndufa1	0.66	0.73	mt-Nd1	2.07	0.08
Ndufa10	0.96	1.00	mt-Nd2	3.27	0.00
Ndufa11	0.91	0.98	mt-Nd3	8.03	0.00
Ndufa12	0.97	1.00	mt-Nd4	2.14	0.04
Ndufa13	0.74	0.88	mt-Nd5	2.50	0.13
Ndufa2	1.14	0.94	mt-Nd6	3.74	0.00
Ndufa3	0.66	0.70	mt-Cytb	1.94	0.15
Ndufa5	0.87	0.97	mt-Co1	1.56	0.76
Ndufa6	0.90	0.97	mt-Co3	2.04	0.37
Ndufa7	0.78	0.88	mt-Ta	2.16	0.72
Ndufa8	0.89	0.97	mt-Tc	0.94	0.97
Ndufa9	0.86	0.94	mt-Tf	5.12	0.01
Ndufab1	0.75	0.81	mt-Ti	2.16	0.65
Ndufb10	0.84	0.95	mt-Tl1	2.28	0.12
Ndufb11	0.74	0.84	mt-Tl2	0.91	0.95
Ndufb2	2.76	0.00	mt-Tm	1.50	0.81
Ndufb3	0.74	0.84	mt-Tp	1.45	0.93
Ndufb4	0.80	0.87	mt-Tq	2.08	0.78
Ndufb5	0.77	0.86	mt-Tr	1.10	1.00
Ndufb6	0.84	0.92	mt-Ts2	0.99	0.98
Ndufb7	0.90	0.98	mt-Tt	2.63	0.05
Ndufb8	0.94	0.99	mt-Tv	1.39	0.91
Ndufb9	0.89	0.98	mt-Rnr1	2.26	0.15
Ndufc1	0.62	0.47	mt-Rnr2	0.81	0.96
Ndufc2	0.80	0.87			
Ndufs1	0.75	0.83			
Ndufs2	0.78	0.89			
Ndufs3	1.02	1.00			
Ndufs4	0.84	0.92			
Ndufs5	0.73	0.81			
Ndufs6	0.69	0.77			
Ndufs7	0.81	0.92			
Ndufs8	1.01	1.00			
Ndufv1	0.74	0.86			
Ndufv2	0.82	0.90			
Ndufv3	0.94	1.00			
Sdha	0.78	0.89			
Sdhb	0.77	0.88			
Sdhc	0.71	0.81			
Sdhd	1.05	0.98			
Cyc1	0.85	0.95			
Uqcr10	0.73	0.83			
Uqcr11	0.75	0.92			
Uqcrb	0.72	0.82			
Uqcrc1	0.88	0.96			

Table S1

Table S1. Related to Figure 1.

nDNA Gene	Fold Δ	p adj
Uqcrc2	1.25	0.88
Uqcrfs1	0.84	0.94
Uqcrh	1.13	0.95
Uqcrq	0.73	0.83
Cox4i1	0.80	0.94
Cox4i2	1.11	0.96
Cox5a	0.91	0.99
Cox5b	0.97	0.99
Cox6a1	0.85	0.95
Cox6a2	0.84	0.95
Cox6b1	0.71	0.79
Cox6c	0.83	0.94
Cox7a1	0.66	0.77
Cox7a2	0.58	0.41
Cox7b	0.78	0.90
Cox7c	0.65	0.84
Cox8a	0.80	0.89
Atp5a1	0.87	0.96
Atp5b	0.74	0.88
Atp5c1	1.02	0.99
Atp5d	0.95	1.00
Atp5e	0.71	0.81
Atp5f1	0.87	0.95
Atp5g1	1.08	0.97
Atp5g3	1.02	1.00
Atp5h	0.89	0.97
Atp5j	0.73	0.83
Atp5j2	0.83	0.94
Atp5l	0.92	1.00
Atp5o	0.77	0.85
Atpif1	1.08	0.97

Table S1

Table S2. Related to Figure 3.

ECG Measure	WT Mean	WT S.D.	COI Mean	COI S.D.	ND6 Mean	ND6 S.D.	ANT1 Mean	ANT1 S.D.	COI ANT1 Mean	COI ANT1 S.D.	ND6 ANT1 Mean	ND6 ANT1 S.D.
SepTd	0.73	0.09	0.74	0.13	0.77	0.11	0.97*	0.12	0.95*	0.13	0.86	0.13
LVEDD	4.25	0.33	4.33	0.25	4.25	0.32	5.22*	0.44	5.51*	1.10	6.62*◆	0.95
PWTd	0.75	0.10	0.79	0.11	0.81	0.12	1.02*	0.14	0.91*	0.13	0.86*◆	0.14
SepTs	1.05	0.13	1.10	0.20	1.05	0.17	1.20*	0.12	1.16*	0.16	1.02	0.15
LVSED	3.07	0.30	3.05	0.25	3.03	0.38	4.30*	0.53	4.67	1.34	6.17*◆	0.98
PWTs	1.07	0.16	1.13	0.17	1.13	0.11	1.29*	0.25	1.09◆	0.22	1.03◆	0.13
FS	27.64	3.24	29.54	3.71	28.79	4.46	17.87*	5.20	16.19*	9.27	7.07*◆	3.18
EF	61.90	5.06	64.74	5.29	63.49	6.51	43.98*	10.23	39.15	18.41	19.49*◆	8.26
LV mass	116.91	22.87	128.20	29.85	127.98	27.49	245.10*	47.11	248.14*	74.84	305.80*◆	70.77
RWT	0.35	0.05	0.37	0.05	0.38	0.07	0.39	0.06	0.34	0.07	0.27*◆	0.06
Global Strain:												
Longitudinal	-13.66	3.70	-13.62	3.06	-11.59	4.53	-7.68*	3.99	-8.87*	4.67	-2.64*◆	1.77
Circumferenctial	-18.33	4.64	-19.38	3.51	-17.44	3.17	-11.25*	3.85	-13.04*	7.89	-4.72*◆	2.12
Radial	23.81	6.93	26.05	8.08	23.98	5.82	17.52*	6.56	17.78*	8.24	8.20*◆	3.30

Table S2